Supporting Information (SI) for the manuscript:

Insights into non-covalent interactions in dicopper(II,II) complexes bearing a naphthyridine scaffold: an anion-dictated electrochemistry

Jonathan De Tovar [a*], Christian Philouze [a], Aurore Thibon-Pourret [a] and Catherine Belle [a]

[a] Univ. Grenoble Alpes, CNRS, UMR 5250, Department of Molecular Chemistry (DCM), 38000 Grenoble, France

Corresponding author: Jonathan.De-Tovar@univ-grenoble-alpes.fr

Table of Contents:

Experimental section

Materials and methods

All reagents were purchased from Sigma-Aldrich, Strem Chemicals, BLDpharm and Fluorochem. All chemical reagents were of analytical grade and were used as received without further purification.

Electrochemical-grade anhydrous acetonitrile was purchased from Acros Organics (99.9% Extra Dry). Ar (99.9999%) employed for electrochemical analyses was purchased from Air Liquide and used without further purification. All the syntheses were carried out under air atmosphere.

^{1}H NMR (400 MHz), ^{13}C{^{1}H} (100 MHz) and 2D NMR spectra were recorded on a Bruker Avance III 400 MHz spectrometer in suitable solvent, and spectra were referenced to residual solvent (^{1}H). The infrared spectra were recorded on an Agilent Technologies Cary 630 FTIR spectrometer equipped with a standard transmission module, a diamond ATR one, and a DialPath sample interface.

The mass spectra were recorded either on an Amazon speed ion trap spectrometer or a LTQ Orbitrap XL type Thermo Scientific spectrometer, both equipped with an electrospray ionization source (ESI). The samples were analyzed in both positive and negative ionization modes by direct perfusion in the ESI-MS interface (ESI capillary voltage = 2kV, sampling cone voltage = 40 V). High-resolution spectra were recorded

Electrochemical experiments were performed using a SP-300 Bio-Logic bipotentiostat in an air-tight cell in the three electrode configuration. Cyclic voltammograms (CV) were recorded using a Ø 3.0 mm glassy carbon disk working electrode, a Pt wire as counter electrode and a $Ag/AgNO_3$ (0.01 M) as reference electrode separated from the bulk solution by a Vycor frit. Experiments were performed under argon using 1 mM solutions of the complexes (3 mL) in anhydrous acetonitrile containing 0.1 M tetrabutylammonium perchlorate [*n*-Bu_4N]ClO_4. Cyclic voltammograms were collected at a scan rates ranging from 10 to 1000 mV s^{-1} at room temperature (298 K). The working electrode was polished before each measurement on a MD-Nap polishing pad with a 1 µm monocrystalline diamond paste, rinsed with ethanol and dried under air. In all experiments, ferrocene was added at the end of electrochemical experiments as an internal standard.

Infrared (IR) spectra were recorded with a Thermo Scientific Nicolet iS10 spectrometer in the 4000-450 cm^{-1} range in attenuated total reflectance (ATR) mode.

EPR analyses were performed at 100 K under a fixed frequency of 9.4284 GHz with an EMX Bruker spectrometer equipped with a standard ER4102ST Bruker cavity, an ESR900 continuous-flow Oxford Instrument cryostat and an ER4131VT Bruker temperature controller. All spectra were recorded under non-saturating conditions. EPR simulations and fittings were carried out with MATLAB 2016b (MathWorks, Natick, MA, USA) using EasySpin[1] and Simultispin[2] toolboxes.

The viscosity of the electrolyte solution was determined at 298.15 K by an Ubbelohde viscometer (type 532) according to the following the equation (1):

$$\eta = K\rho(t - \vartheta) \qquad (1)$$

where K and ϑ are the Ubbelohde constant and Hagenbach correction, respectively, whose are equal to 0.01 and 1.03 for the used Ubbelohde viscometer, and ρ is the density of the solution.

For observed irreversible behaviors, first, the symmetry factor of the electron transfer α_r is determined by plotting the intensity of the anodic peak I_{pa} versus different square roots of scan rate according to Bard *et al.*[3] (Equations (2) and (3)).

$$I_{pa} = -0.496AnFC_A^*\sqrt{\alpha_r nf\nu D_A}; f = \frac{F}{RT} \quad (2)$$

$$E_{pa} = E^0 + \frac{1}{\alpha_r nf}\left(-0.78 + ln\frac{k^0}{\sqrt{\alpha_r nf\nu D_A}}\right); f = \frac{F}{RT} \quad (3)$$

With *F*, the Faraday constant (96485 C mol^{-1}), *R* the perfect gas constant (8.314 J K^{-1} mol^{-1}), *T* the ambient temperature (298 K), C_A* the bulk concentration of species A (**C1·(X)$_2$** or **C2**) in mol cm^{-3}, *n* the number of exchanged electrons, D_A the diffusion coefficient of species A in cm^2 s^{-1} and ν the scan rate in V s^{-1}.

Equation (3) can be written as an affine law:

$$E_{pa} = aln\nu + E_{oo} \quad (4)$$

With E_{oo} the ordinate at the origin of the E_{pa} vs $ln\ \nu$ curve and *a* its slope.

$$a = \frac{1}{2\alpha_r nf} \Longrightarrow n = \frac{1}{2\alpha_r af}$$

Using the slope *a*, we can directly get the number of exchanged electrons *n* in such a redox process.

Diffusion coefficients were calculated according to the Randles-Ševčík equation (5):

$$i_{pa} = 269000 \cdot D^{1/2} \cdot n^{3/2} \cdot A \cdot [C] \cdot \nu^{1/2} \quad (5)$$

where i_{pa} is the oxidation peak current for each complex, *n* is the number of electrons involved in the transfer, *A* is the electrode area, *D* is the diffusion coefficient, *[C]* is the complex concentration and ν is the scan rate.

Hydrodynamic radii were calculated by the Stokes-Einstein equation (6):

$$D = \frac{k_B T}{6\pi\eta_e r_H} \quad (6)$$

in which k_B is the Boltzmann constant, "T" is the absolute temperature, η_e is the electrolyte-containing solvent viscosity and r_H is the hydrodynamic radius. Note that we consider the molecular volumes of the complexes as a hard spheres leading only to comparative r_H values under these conditions.

Suitable single crystals were mounted on a Bruker AXS-Enraf Nonius-kappa APEX II diffractometer equipped with an Incoatec high brilliance microsource with multilayer monochromated mirrors. The crystals were kept at a steady T = 200.00 K using an Oxford cryosystem during data collection. Data were measured using MoK_α radiation (λ = 0.71073 Å) and collected using phi and omega scans. Cell determination and refinement were performed using Bruker AXS "Collect" program. Data integration was made with EvalCCD.[4] Data reduction was undertaken with Xprep software. The structures were solved with the SheIXT[5] structure solution program using Intrinsic Phasing solution method and by using Olex2[6] as a graphical interface. The models were refined with SheIXL[7] using Least Squares minimization. Hydrogen atoms were calculated geometrically for all structures.

Synthetic scheme followed in this work

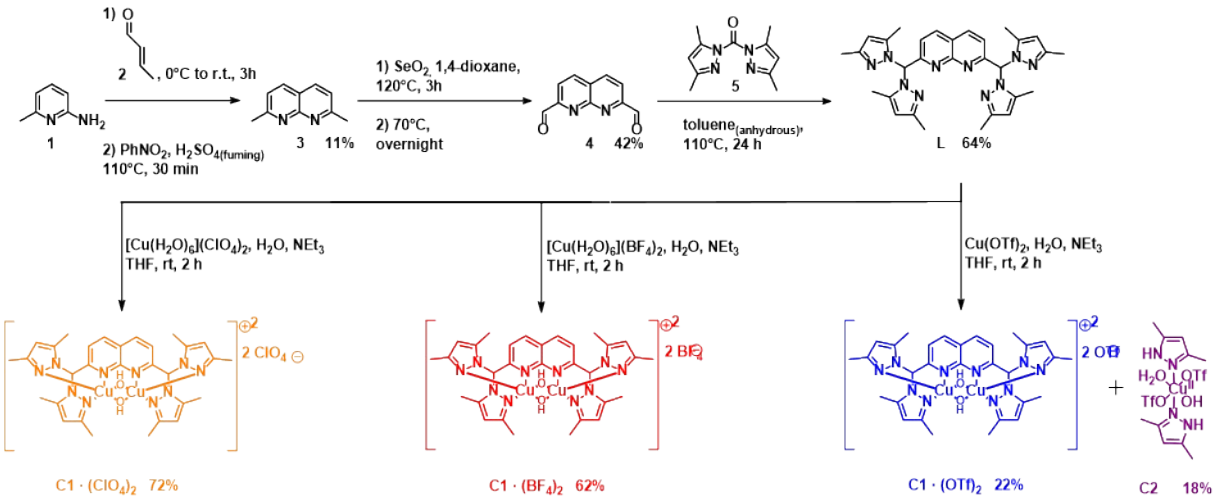

Scheme S1. Synthetic scheme for the preparation of **L** ligand and **C1·(ClO$_4$)$_2$**, **C1·(BF$_4$)$_2$** and **C1·(OTf)$_2$** complexes.

Synthesis of Ligands

***Synthesis of 1,8-naphthyridine-2,7-bis(bis-3,5-dimethylpyrazolemethane)* (*L*).** A sealed Schlenk was charged with a suspension of anhydrous toluene (3 mL) containing **4** (100 mg, 0.54 mmol, 1 eq) and **5** (235 mg, 1.07 mmol, 2 eq) and was further stirred at 110°C for 24 h under argon. The resulting reddish solution was evaporated. Then, flash chromatography column using ethyl acetate : hexane (2 : 1) was performed. After removing the solvent mixture, the title compound was obtained as a hygroscopic brown-orange powder. Yield: 184 mg, 65%. ^{1}H NMR (CD$_3$CN, 400 MHz, 25°C): δ 2.14 (s, 12H, H$_9$), 2.19 (s, 12H, H$_8$), 5.96 (s, 4H, H$_6$), 7.39 (d, *J* = 8.48 Hz, 2H, H$_2$), 7.75 (s, 2H, H$_4$), 8.40 (d, *J* = 8.50 Hz, 2H, H$_1$). ^{13}C{^{1}H} NMR (CD$_3$CN, 100 MHz, 25°C): δ 11.2 (C$_8$), 13.5 (C$_9$), 74.9 (C$_4$), 107.3 (C$_6$), 122.3 (C$_2$), 138.7 (C$_1$), 141.8 (C$_5$), 149.0 (C$_7$), 154.8 (C$_{11}$), 160.5 (C$_3$). IR (ATR) cm^{-1}: 2955 ν(C-H)ar, 2925 ν(C-H), 1458 δ(C=C), δ(C=N)ar, 1255 ν(C-N)ar, 1077 δ(C-H)ip, 1028 δ(C-H)ip, 806 δ(C-H)oop. HR-ESI-MS (MeOH) calculated: m/z = 535.30407 ([M + H]$^+$); Found 535.30269 ([M + H]$^+$). ESI-MS (MeOH) calculated: m/z = 535.30 ([M + H]$^+$); Found 535.33 ([M + H]$^+$).

Synthesis of Complexes

***Synthesis of* C1·(ClO$_4$)$_2$.** A solution of copper(II) perchlorate hexahydrate (36 mg, 0.1 mmol, 2.1 eq) in THF (2 mL) was added to a solution of **L** (25 mg, 0.05 mmol, 1 eq) in THF (2 mL). The reaction mixture changed from orange to green. Then, triethylamine (35 µL, 0.25 mmol, 5.4 eq) was added and the solution became dark green. After stirring for 1 h, the reaction was filtered and layered with diisopropyl ether (3 mL) until a green oil appears on the vessel walls. Then, after removing the blurry solvent and washing the green oil with diisopropyl ether (2 x 2 mL), acetone (2 mL) was added yielding a blue solution. The latter was layered with diisopropyl ether and yielded pale blue crystals. Yield: 30 mg, 72 %. HR-ESI-MS (CH$_3$CN) calculated: m/z = 347.08019 ([M – 2 ClO$_4^-$]$^{2+}$); Found 347.07978 ([M – 2 ClO$_4^-$]$^{2+}$). ESI-MS (CH$_3$CN) calculated: m/z = 347.08 ([M – 2 ClO$_4^-$]$^{2+}$); Found 347.13 ([M – 2 ClO$_4^-$]$^{2+}$). IR (ATR) cm^{-1}: 3402 ν(O-H), 2943 ν(C-H)ar, 2925 ν(C-H), 1604 δ(C=C)ar, δ(C=N)ar, 1251 ν(C-N)ar, 1076 δ(C-H)ip, 808 δ(C-H)oop.

***Synthesis of* C1·$(BF_4)_2$.** A solution of copper(II) tetrafluoroborate hexahydrate (68 mg, 0.2 mmol, 2.1 eq) in THF (4.6 mL) was added to a solution of **L** (50 mg, 0.09 mmol, 1 eq) and water (17 µL, 0.9 mmol, 10 eq) in THF (4.6 mL). The reaction mixture changed from orange to green. Then, triethylamine (35 µL, 0.25 mmol, 5.4 eq) was added and the solution became dark green. The reaction mixture was stirred for 2 h. Then, after removing the solvent under vacuum, dichloromethane (2 mL) was added to the reaction crude which was further filtered through celite. After that, acetonitrile (2 mL) was added to the celite cake solubilizing the title compound. Finally, acetone (1 mL) was added to the celite cake filtrate and layered with diisopropyl ether to afford turquoise crystals (**C1·$(BF_4)_2$**). Yield: 50 mg, 62 %. HR-ESI-MS (CH_3CN) calculated: m/z = 347.08019 ($[M - 2\ BF_4]^{2+}$); Found 347.07987 ($[M - 2\ BF_4]^{2+}$). IR (ATR) cm^{-1}: 3534 ν(O-H), 2991 ν(C-H)ar, 2940 ν(C-H), 1608 δ(C=C)ar, δ(C=N)ar, 1310 ν(C-N)ar, 1034 δ(C-H)ip, 799 δ(C-H)oop.

***Synthesis of* C1·$(OTf)_2$.** A solution of copper(II) triflate (71 mg, 0.2 mmol, 2.1 eq) in THF (4.6 mL) was added to a solution of **L** (50 mg, 0.09 mmol, 1 eq) and water (17 µL, 0.9 mmol, 10 eq) in THF (4.6 mL). The reaction mixture changed from orange to green. Then, triethylamine (35 µL, 0.25 mmol, 5.4 eq) was added and the solution became dark green. The reaction mixture was stirred for 2 h forming a cloudy solution. The latter was filtered through a PFTE filter and layered with diisopropyl ether to yield green crystals. Yield: 20 mg, 22 %. HR-ESI-MS (CH_3CN) calculated: m/z = 347.08019 ($[M - 2\ OTf]^{2+}$); Found 347.07984 ($[M - 2\ OTf]^{2+}$). ESI-MS (CH_3CN) calculated: m/z = 1141.02 ($[M + OTf]^-$), 843.11 ($[M - OTf]^+$), 347.08 ($[M - 2\ OTf]^{2+}$); Found 1140.91 ($[M + OTf]^-$), 843.07 ($[M - OTf]^+$), 347.09 ($[M - 2\ OTf]^{2+}$). IR (ATR) cm^{-1}: 3429 ν(O-H), 2978 ν(C-H)ar, 2921 ν(C-H), 1434 δ(C=C), δ(C=N)ar, 1249 ν(C-N)ar, 1026 δ(C-H)ip.

***Synthesis of* C2.**

The PFTE filter cake from the synthesis of **C1·$(OTf)_2$** was rinsed with dichloromethane (5 mL) giving a green solution. Slow evaporation of the latter gave **C2** as green crystals. Yield: 19 mg, 18 %. IR (ATR) cm^{-1}: 3328 ν(O-H), 2946 ν(C-H)ar, 1480 δ(C=C), δ(C=N)ar, 1230 ν(C-N)ar, 1028 δ(C-H)ip, 1028 δ(C-H)ip, 798 δ(C-H)oop.

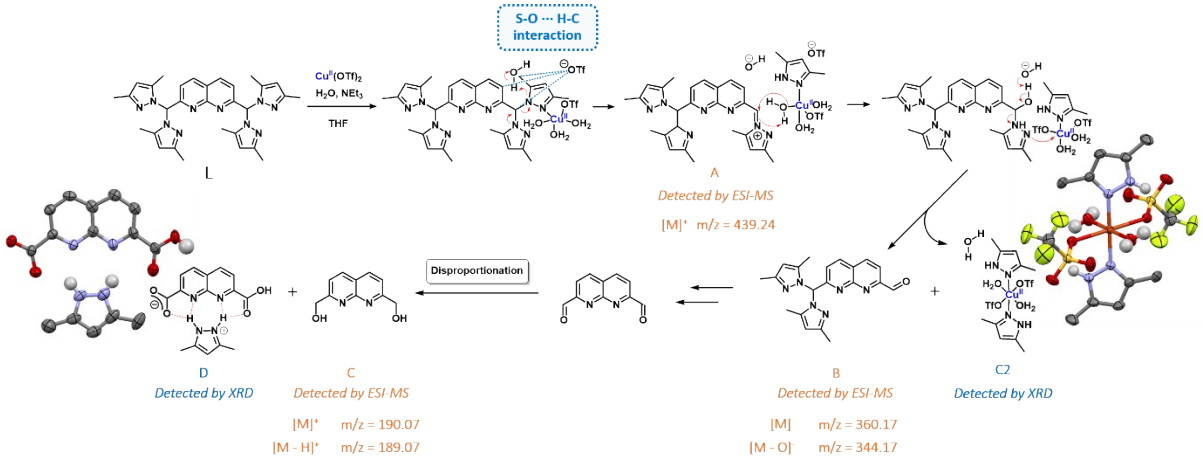

Scheme S2. Proposed mechanism for the formation of **A**, **B**, **C**, **D** and **C2** and displacement ellipsoid plots of **C2** and **D** at the 50% probability level. Solvent molecules and hydrogen atoms (except for the 3,5-dimethylpyrazolium cation in D and 3,5-dimethylpyrazolo and aqua ligands in **C2**) are omitted for clarity.

As shown in Scheme S2, in this species, the copper center is coordinated by two triflato, two aqua and two 3,5-dimethylpyrazolo ligands all in trans, respectively. From here, it can be inferred that presumably the triflate anions enhance the elimination of the adjacent 3,5-dimethylpyrazole unit forming a dimethylpyrazolium intermediate, which after being deprotonated can release another 3,5-

dimethylpyrazole unit as illustrated by the proposed mechanism in Scheme S2. Furthermore, the **L** ligand resulted to evolve into 3,5-dimethylpyrazolium 1,8-naphthyridine-2,7-dicarboxylate (**D**), as evidenced from its crystals X-ray diffraction analysis (Scheme S2 and Table S2), presumptively through a disproportionation reaction orchestrated by the basic pH of the reaction medium (Scheme S1). Nevertheless, although we did not obtain crystals for the 1,8-naphthyridine-2,7-dimethanol (**C**), its presence has been observed from the ESI-MS spectrum of the crude solution (Fig. S15).

CRediT authorship contribution statement

Jonathan De Tovar: Conceptualization, Validation, Formal analysis, Investigation, Writing – original draft, Writing – review & editing, Visualization. **Christian Philouze:** Data curation, writing – review & editing. **Aurore Thibon-Pourret:** Resources, Validation, Writing – review & editing, Visualization, Project administration, Funding acquisition. **Catherine Belle:** Resources, Validation, Writing – review & editing, Visualization, Project administration, Funding acquisition.

Declaration of Competing Interest

The authors declare no competing financial interests.

Appendix A

CCDC 2312255 (for **C1·(ClO$_4$)$_2$**), 2312256 (for **C1·(BF$_4$)$_2$**), 2312257 (for **C1·(OTf)$_2$**), 2312258 (for **C2**) and 2312259 (for **D**), contain the supplementary crystallographic data for this paper. These data can be obtained free of charge from The Cambridge Crystallographic Data Centre via www. ccdc.cam.ac.uk/data_request/cif.

Tables:

Table S1. Selected Crystallographic Data for Complexes **C1·(ClO$_4$)$_2$, C1·(BF$_4$)$_2$** and **C1·(OTf)$_2$.**

	C1·(ClO$_4$)$_2$	**C1·(BF$_4$)$_2$** [a]	**C1·(OTf)$_2$**
formula	$C_{36}H_{48}Cl_2Cu_2N_{10}O_{12}$	$C_{37.12}H_{54.51}B_2Cl_{0.37}Cu_2F_8N_{10.38}O_{6.26}$	$C_{40}H_{52}Cu_2F_6N_{10}O_{10}S_2$
formula weight	1010.82	1059.97	1138.11
crystal color	colourless	colourless	green
crystal size (mm^3)	0.28 x 0.24 x 0.08	0.37 x 0.31 x 0.06	0.28 x 0.22 x 0.12
crystal system	Triclinic	Triclinic	Orthorhombic
space group	P-1	P-1	Pnma
a (Å)	11.652(2)	11.5059(10)	13.529(3)
b (Å)	13.232(3)	15.193(2)	20.929(4)
c (Å)	16.020(3)	15.470(2)	16.907(3)
α (deg)	106.82(3)	76.645(9)	90
β (deg)	96.99(3)	73.531(9)	90
γ (deg)	110.12(3)	68.400(7)	90
V (Å^3)	2151.7(9)	2386.7(5)	4787.2(17)
Z	2	2	4
$D_{calc.}$ (g/cm^3)	1.560	1.475	1.579
reflections	9831	10904	5577
μ (mm^{-1})	1.185	0.997	1.065
parameters/restra	686/311	747/397	383/516
R1/wR2 ($I>2\sigma(I)$)	0.0294/0.0742	0.0429/0.1106	0.0409/0.0956
R1/wR2 (all data)	0.0368/0.0804	0.0606/0.1284	0.0626/0.1114
Largest peak and deepest hole (e/Å^3)	0.492/-0.557	1.208/-0.748	0.534/-0.490

[a] *Note that the statistical occupational hydroxido : chlorido disorder ratios 0.91 : 0.08 (O2:Cl2) and 0.72 : 0.28 (O1:Cl1) associated to intercopper bridges in **C1·(BF$_4$)$_2$** are observed, resulting in the coexistence of two species on the same crystallographic positions.*

Table S2. Selected Crystallographic Data for **C2** and **D**.

	C2	**D**
formula	$C_{12}H_{20}CuF_6N_4O_8S_2$	$C_{15}H_{20}N_4O_7$
formula weight	598.98	368.35
crystal color	green	colourless
crystal size (mm^3)	0.30 x 0.26 x 0.25	0.18 x 0.13 x 0.12
crystal system	Monoclinic	Monoclinic
space group	$P2_1/c$	$P2_1/c$
a (Å)	10.686(2)	11.301(2)
b (Å)	14.011(3)	23.093(5)
c (Å)	8.0619(16)	6.9978(14)
α (deg)	90	90
β (deg)	110.87(3)	105.89(3)
γ (deg)	90	90
V ($Å^3$)	1127.8(4)	1756.4(7)
Z	2	4
$D_{calc.}$ (g/cm^3)	1.737	1.393
reflections	2574	3082
μ (mm^{-1})	1.249	0.112
parameters/restraints	211/165	312/203
R1/wR2 ($I>2\sigma(I)$)	0.0279/0.0782	0.0972/0.2889
R1/wR2 (all data)	0.0325/0.0841	0.1134/0.3039
Largest peak and deepest hole ($e/Å^3$)	0.407/-0.301	0.409/-0.272

Table S3. Selected Bond Lengths (Å) and Angles (deg) for Complexes **C1·$(ClO_4)_2$, C1·$(BF_4)_2$, C1·$(OTf)_2$**.

	C1·$(ClO_4)_2$	**C1·$(BF_4)_2$**	**C1·$(OTf)_2$**
Cu1-N_{naph}1	2.327(2)	2.370(2)	2.338(2)
Cu2-N_{naph}2	2.279(2)	2.551(2)	2.338(2)
Cu1-Cu2	2.785(1)	2.9051(5)	2.7877(8)
Cu1-O5 (copper – acetone)	-	2.793(3)	-
Cu2-O3 (copper – aqua)	-	2.324(3)	-
Ligand bend[a]	4.01° - 4.47°	3.37° - 4.07°	8.13°

[a] Ligand bend = angle between naphthyridine and N_{naph}1Cu1Cu2N_{naph}2 planes.

Table S4. Peak potentials, symmetry factors, exchanged electrons, hydrodynamic radii and diffusion coefficients in anhydrous acetonitrile containing 0.1 M [*n*-Bu_4N]ClO_4 at 298 K.

Entry	**Complex**	**E_{pa} (V vs $Fc^{+/0}$)**	**α_r**	**n**	**M_w (g mol^{-1})**	**r_H (Å)**	**D (cm^2 s^{-1})**
1	**C1·$(ClO_4)_2$**	1.36	0.5	0.95	894.67	21.89	$2.8 \cdot 10^{-6}$
2	**C1·$(BF_4)_2$**	1.57	0.5	1.24	869.39	13.11	$4.6 \cdot 10^{-6}$
3	**C1·$(OTf)_2$**	1.63	0.5	1.18	993.9	21.55	$2.8 \cdot 10^{-6}$
4	**C2**	1.64	0.5	0.87	589.97	2.44	$2.5 \cdot 10^{-5}$

Table S5. Parameters obtained from EPR simulations.

Entry	Complex	$g_{\parallel}$	$g_{\perp}$	$A_{\parallel}$ / mT	$A_{\perp}$ / mT
1	**C1 · $(ClO_4)_2$ oxidized**	2.250	2.115 (g_x), 2.057 (g_y)	16.41	0.756 (A_x), 0.666 (A_y)
2	**C1 · $(BF_4)_2$ oxidized**	2.263	2.125 (g_x), 2.067 (g_y)	16.00	1.090 (A_x), 0.663 (A_y)
3	**C1 · $(OTf)_2$ oxidized**	2.254	2.119(g_x), 2.069 (g_y)	16.38	0.755 (A_x), 0.662 (A_y)
4	**C2**	2.309	2.064 ($g_x = g_y$)	16.18	-

Figures:

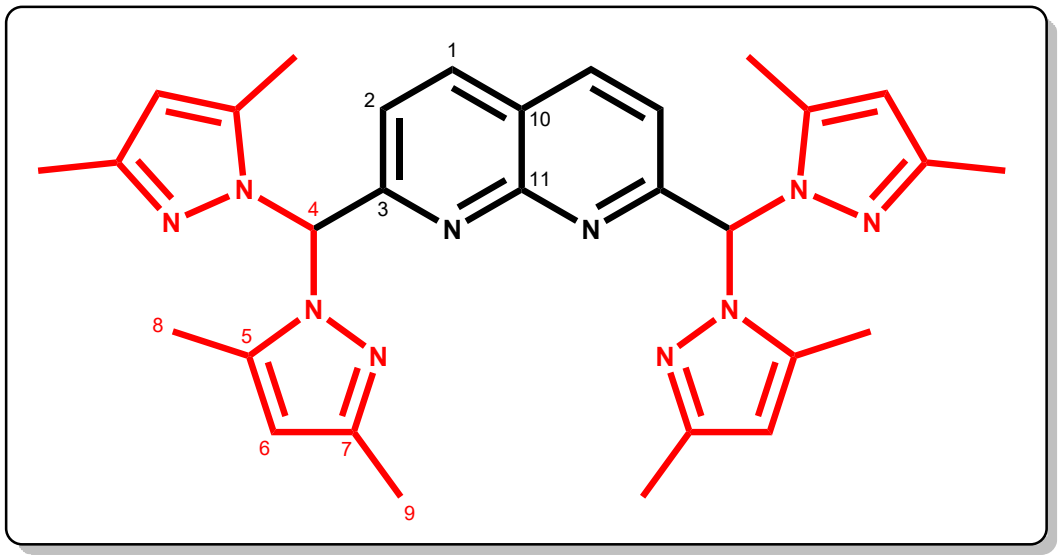
1
2
3
4
5
6
7
8
9
10
11
N
N
N
N
N
N
N
N

(a)

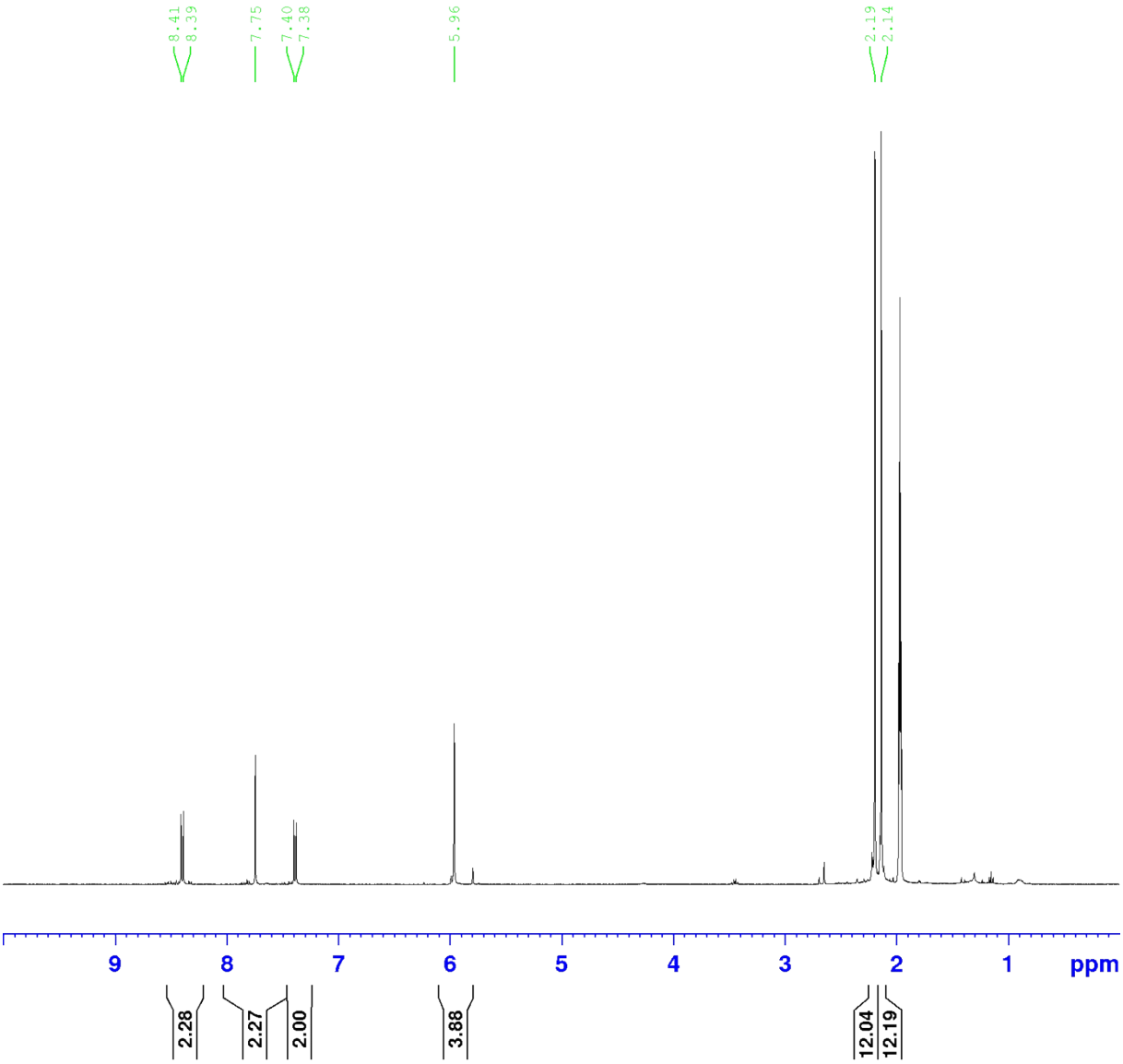
8.41
8.39
7.75
7.40
7.38
5.96
2.19
2.14
9
8
7
6
5
4
3
2
1
ppm
2.28
2.27
2.00
3.88
12.04
12.19

(b)

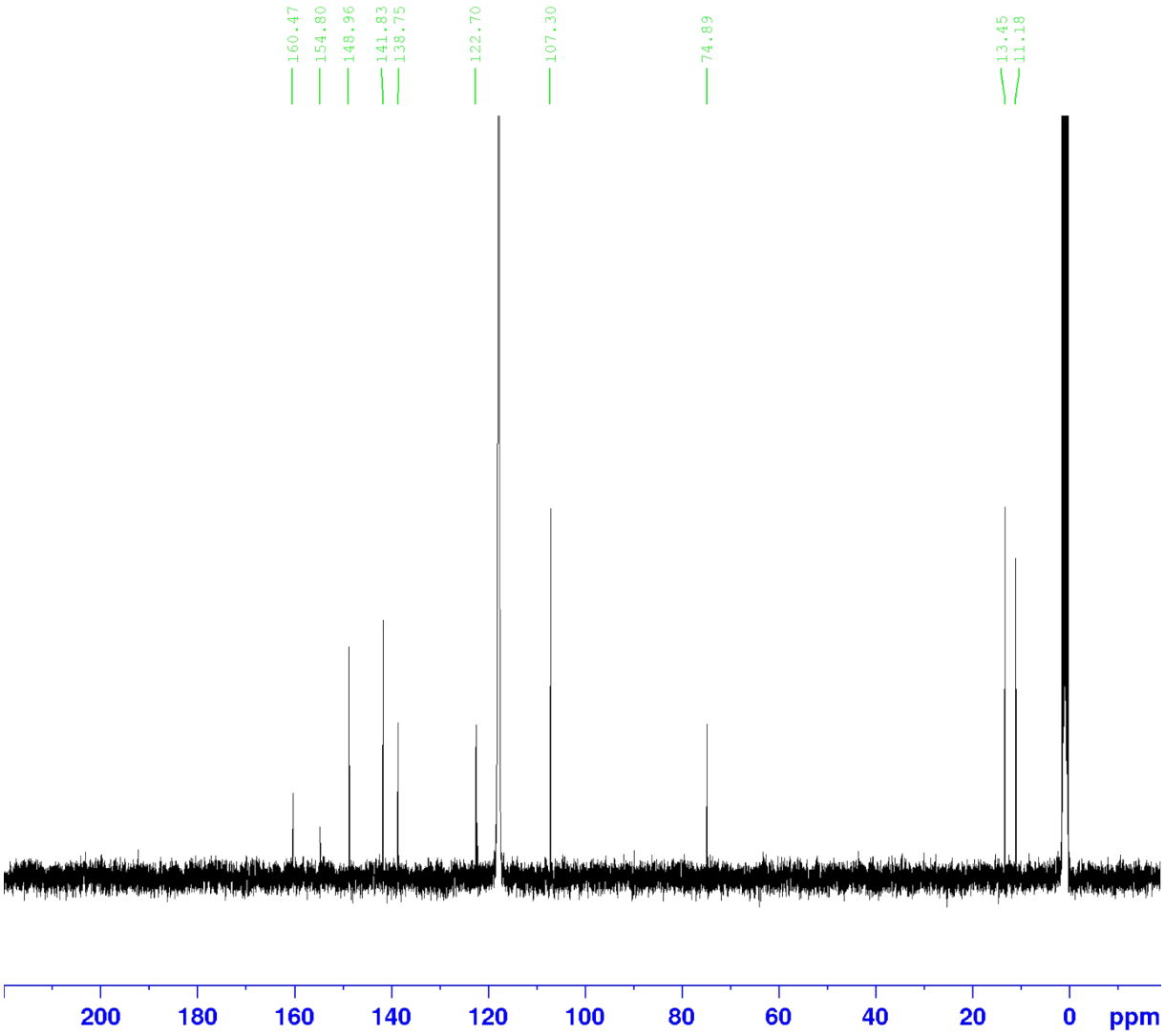
160.47
154.80
148.96
141.83
138.75
122.70
107.30
74.89
13.45
11.18
200
180
160
140
120
100
80
60
40
20
0
ppm

(c)

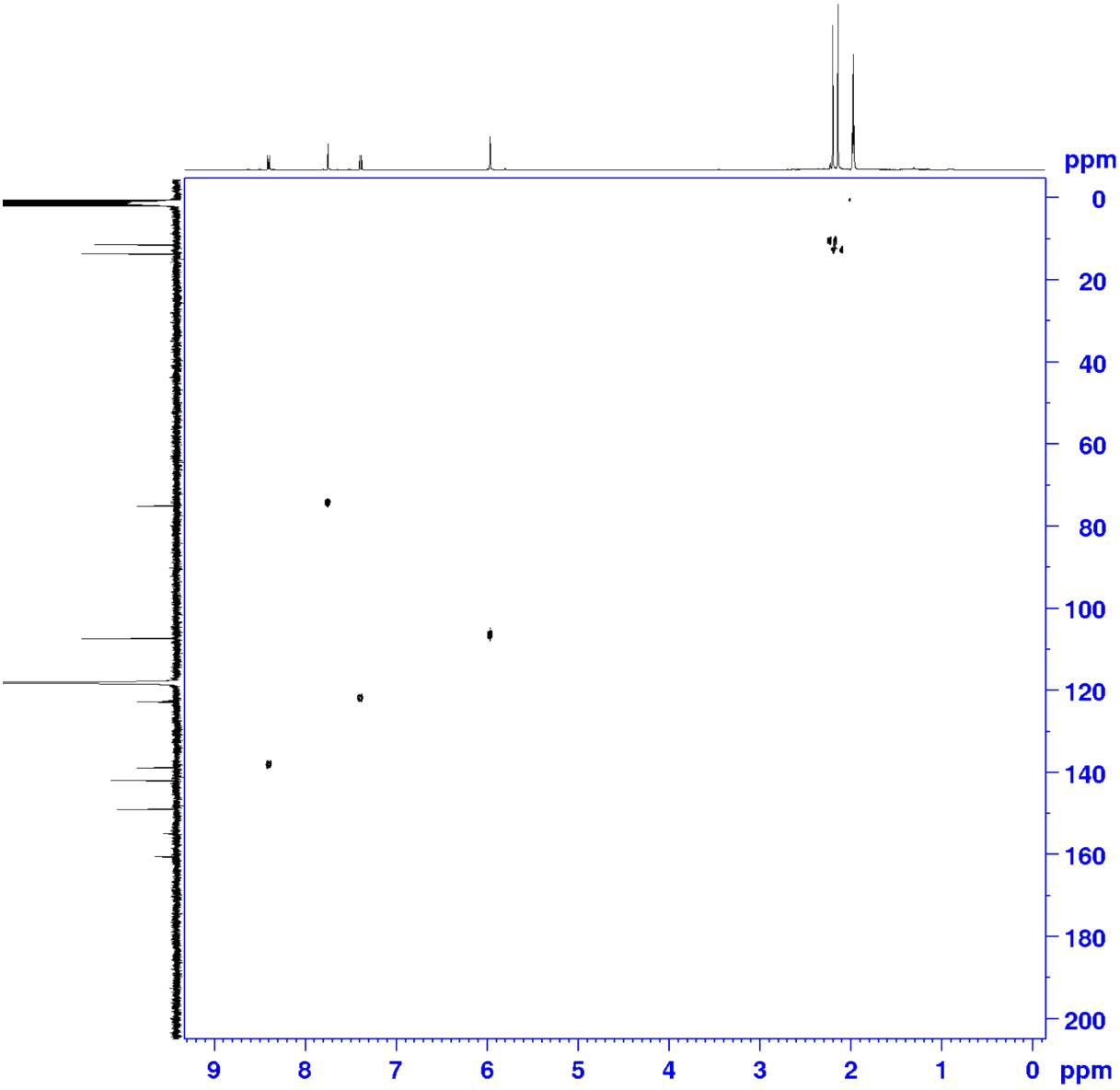

(d)

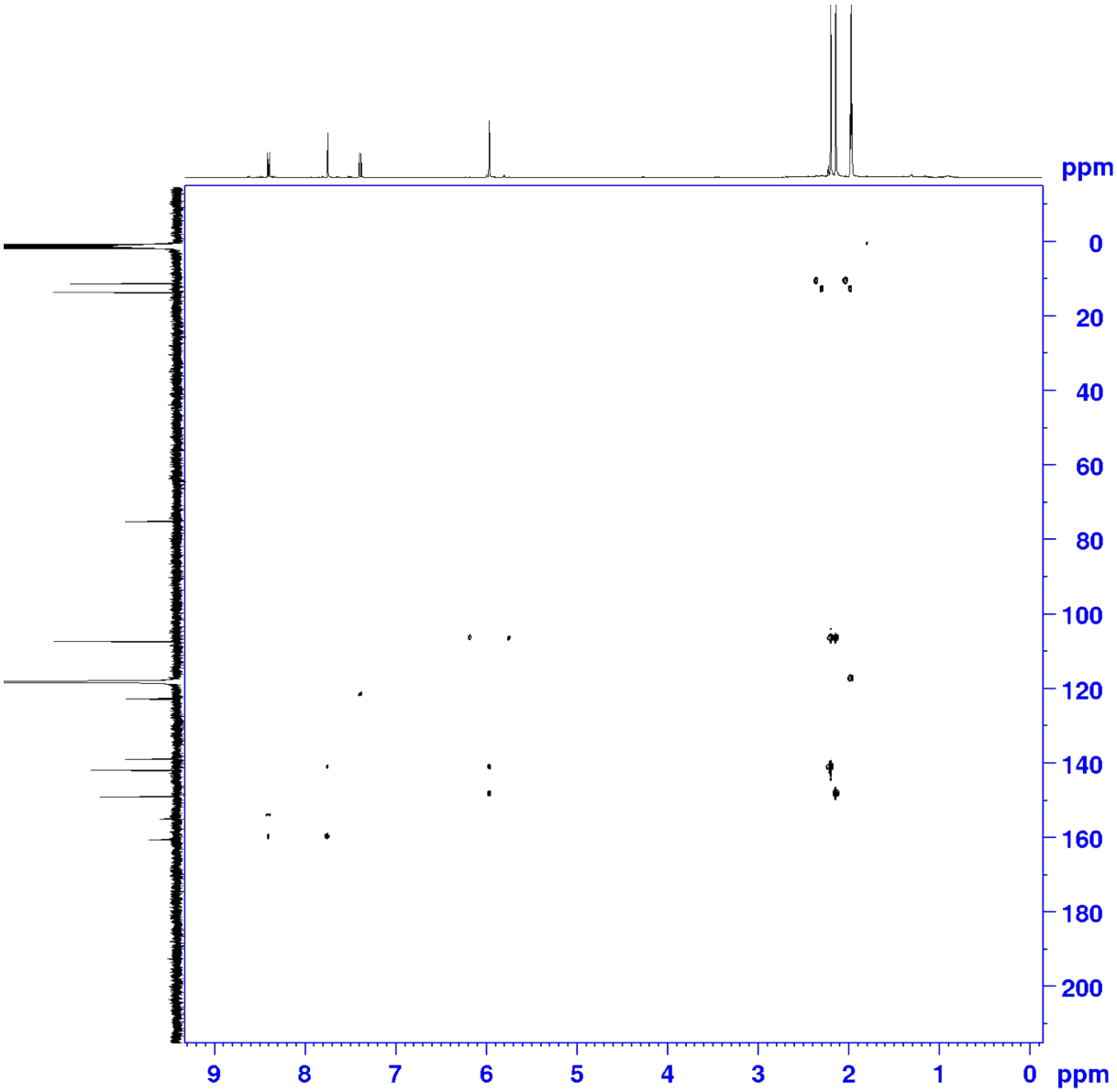

Figure S1. 1D and 2D NMR spectra (400 MHz, 298K, CD_3CN) of **L:** (a) ^{1}H NMR, (b) $^{13}C\{^{1}H\}$ NMR, (c) HSQC NMR, (d) HMBC NMR.

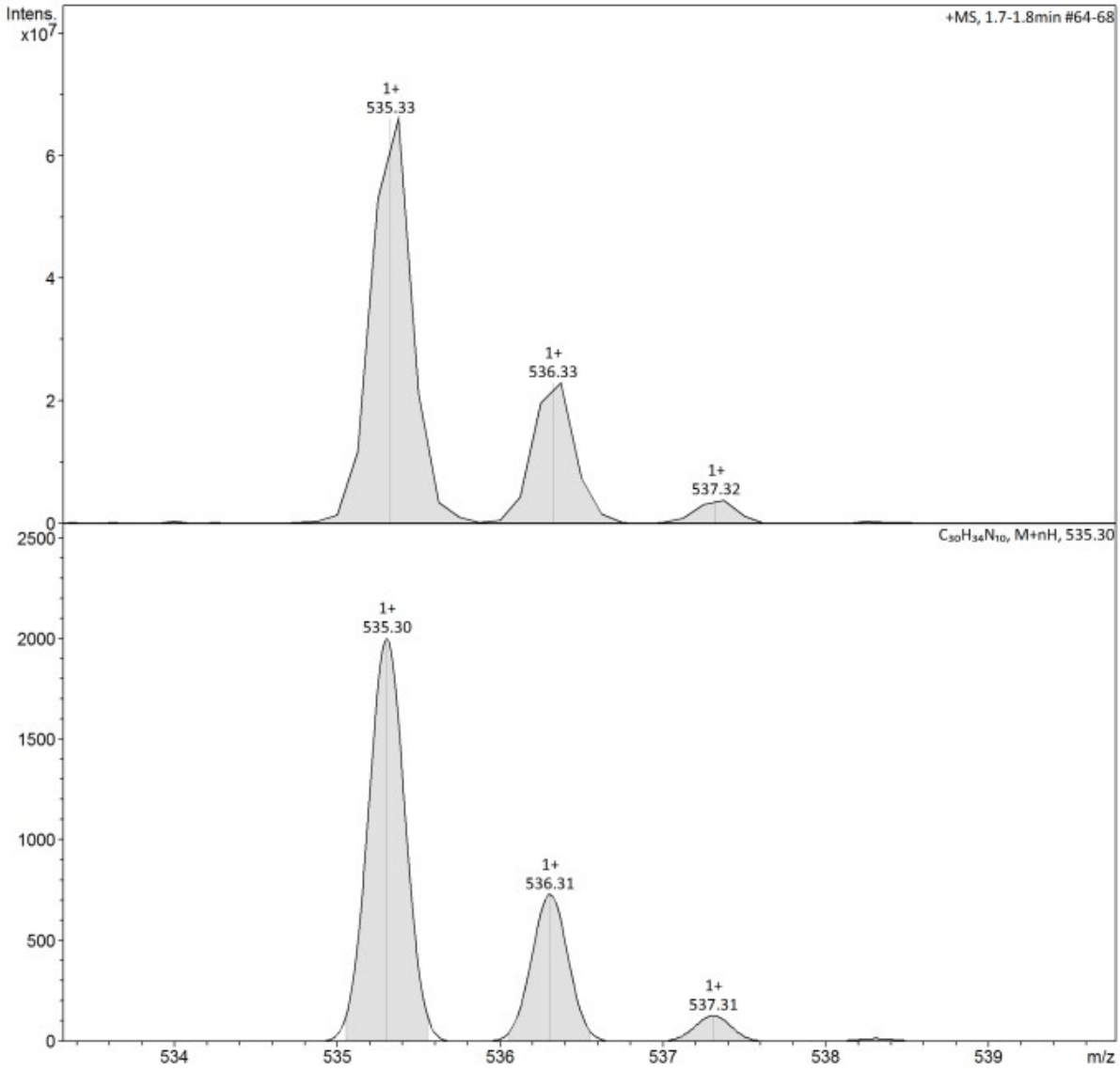

Figure S2. ESI-MS spectrum of **L**. Experimental (top) and simulated (bottom) for the $[M + H]^+$ cation.

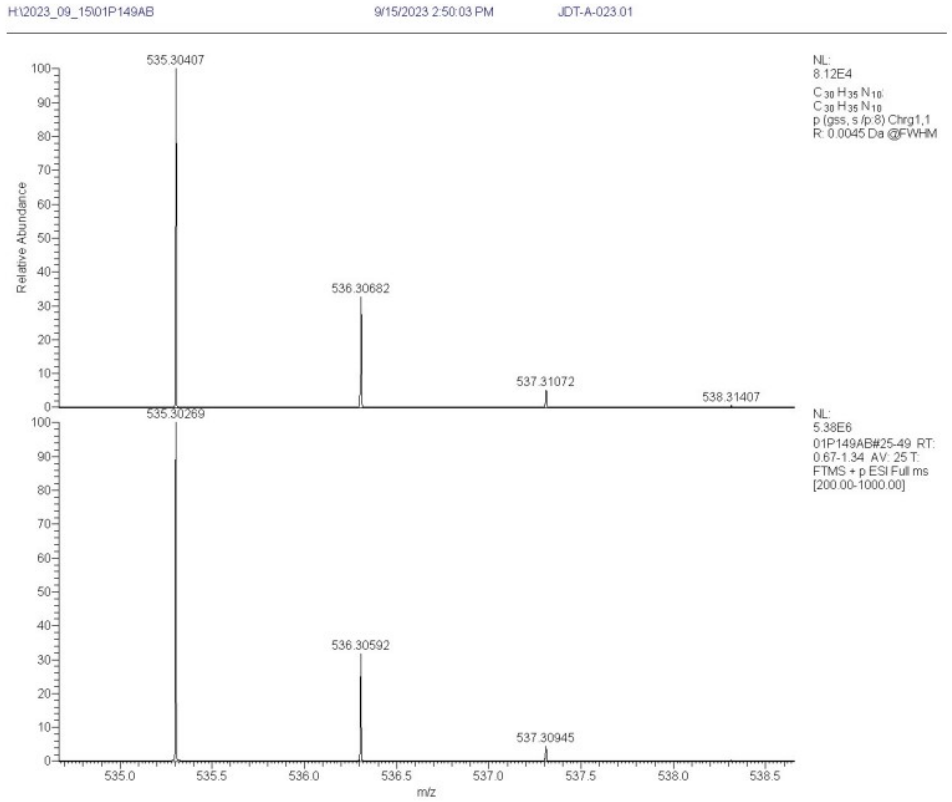

Figure S3. HR-ESI-MS spectrum of **L**. Experimental (top) and simulated (bottom) for the $[M + H]^+$ cation.

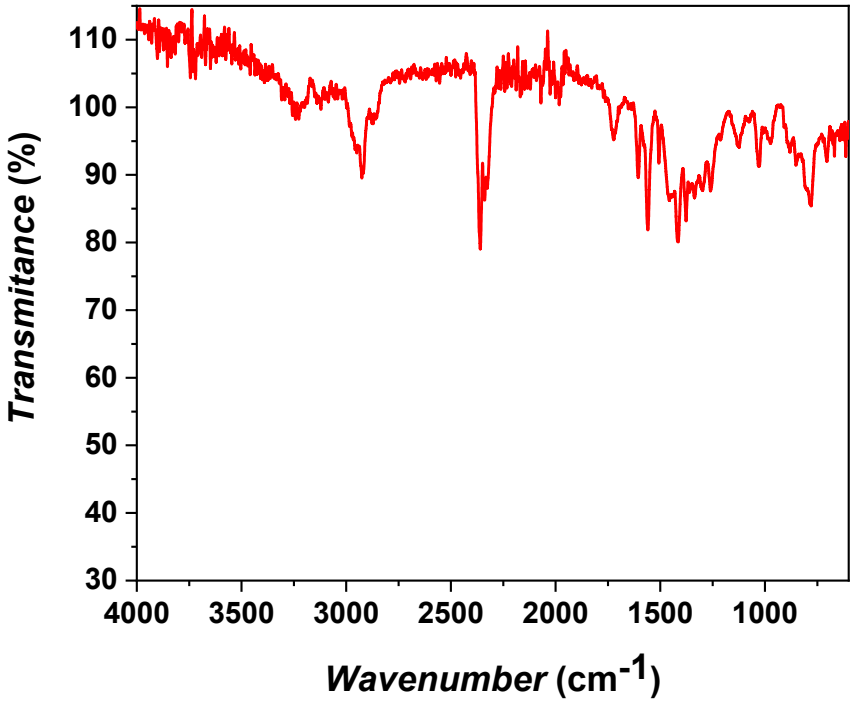

Figure S4. IR-ATR spectrum of **L**.

(a)

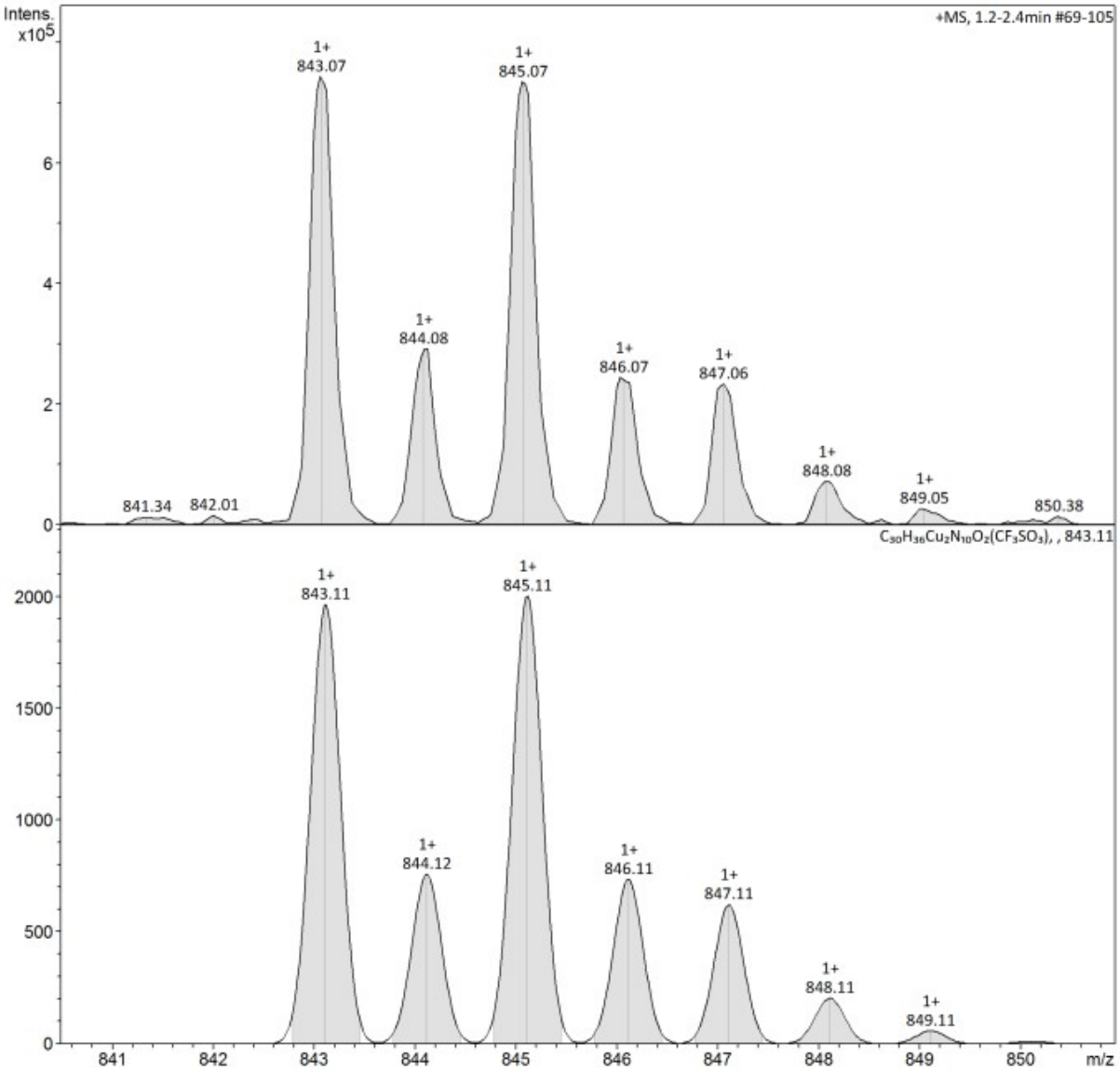
Intens.
x10^5
+MS, 1.2-2.4min #69-105
1+
843.07
1+
845.07
1+
844.08
1+
846.07
1+
847.06
1+
848.08
1+
849.05
841.34
842.01
850.38
C50H36Cu2N10O2(CF3SO3), , 843.11
1+
843.11
1+
845.11
1+
844.12
1+
846.11
1+
847.11
1+
848.11
1+
849.11
m/z

b)

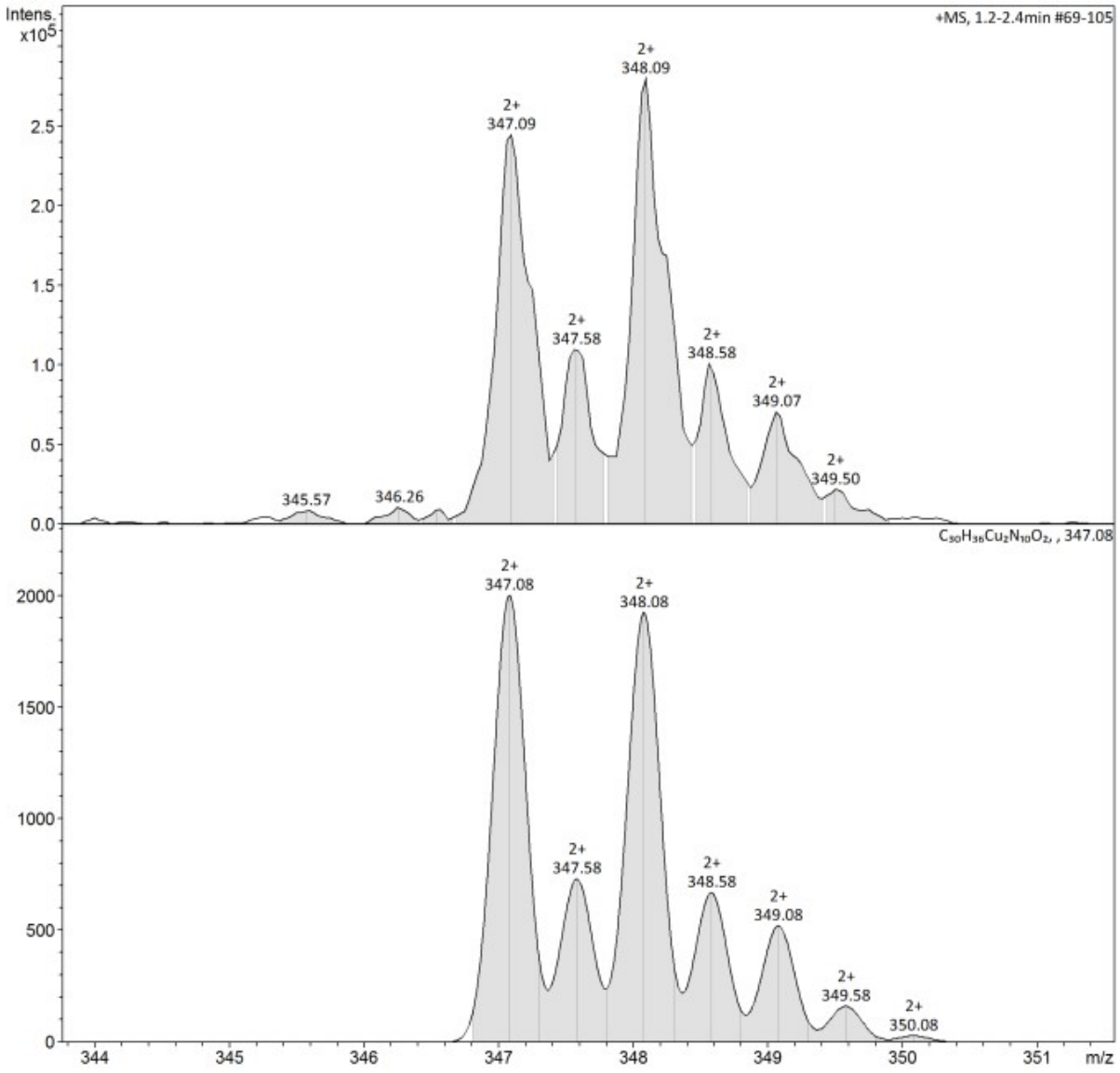
Intens.
x10^5
+MS, 1.2-2.4min #69-105
2+
348.09
2+
347.09
2+
347.58
2+
348.58
2+
349.07
2+
349.50
345.57
346.26
C50H36Cu2N10O2, , 347.08
2+
347.08
2+
348.08
2+
347.58
2+
348.58
2+
349.08
2+
349.58
2+
350.08
m/z

c)

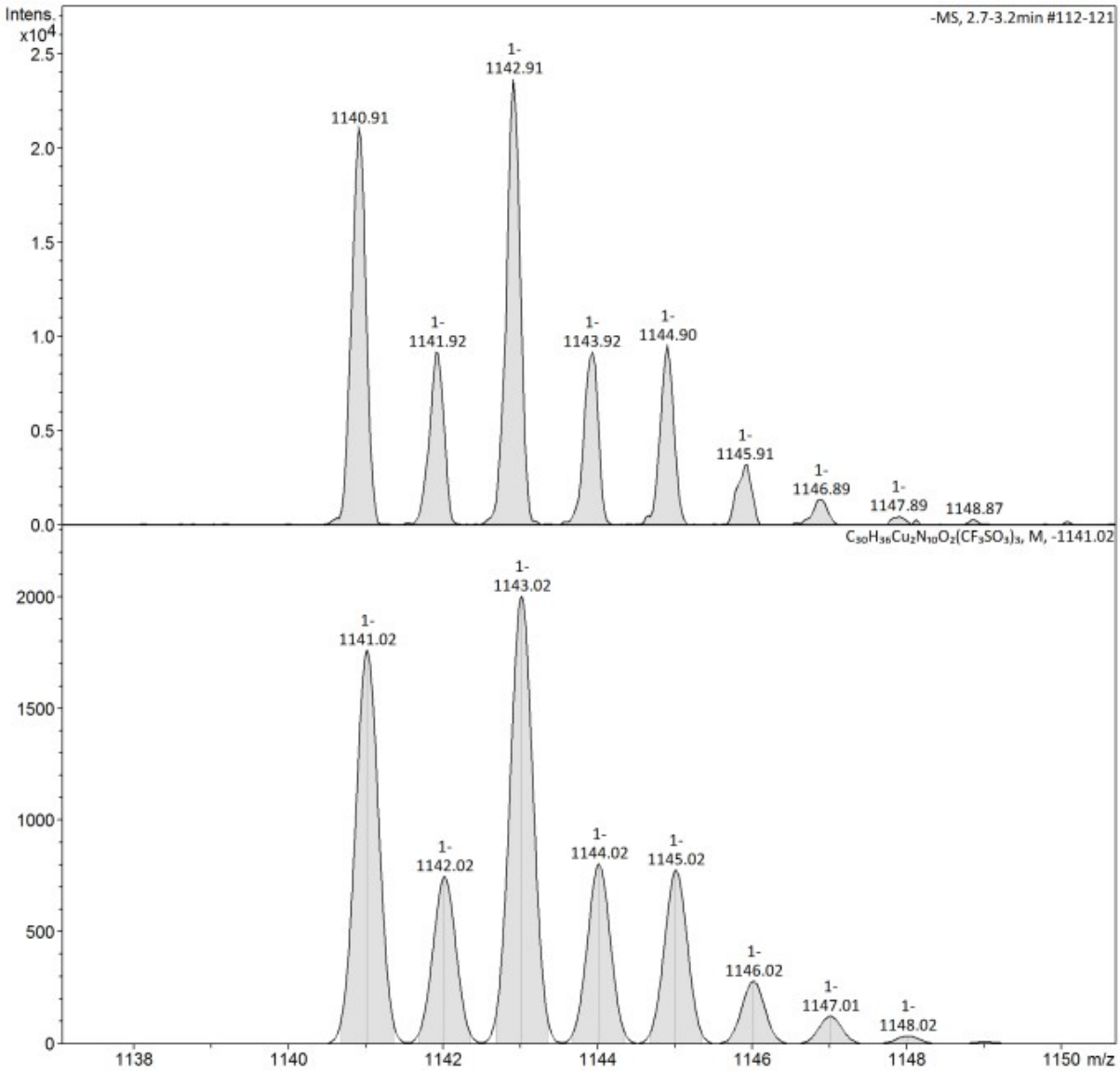

Figure S5. ESI-MS spectrum of **C1·(OTf)$_2$**. Experimental (top) and simulated (bottom) for the a) [M - OTf]$^+$ cation, b) [M – 2 OTf]$^{+2}$ cation and c) [M + OTf]$^-$ anion.

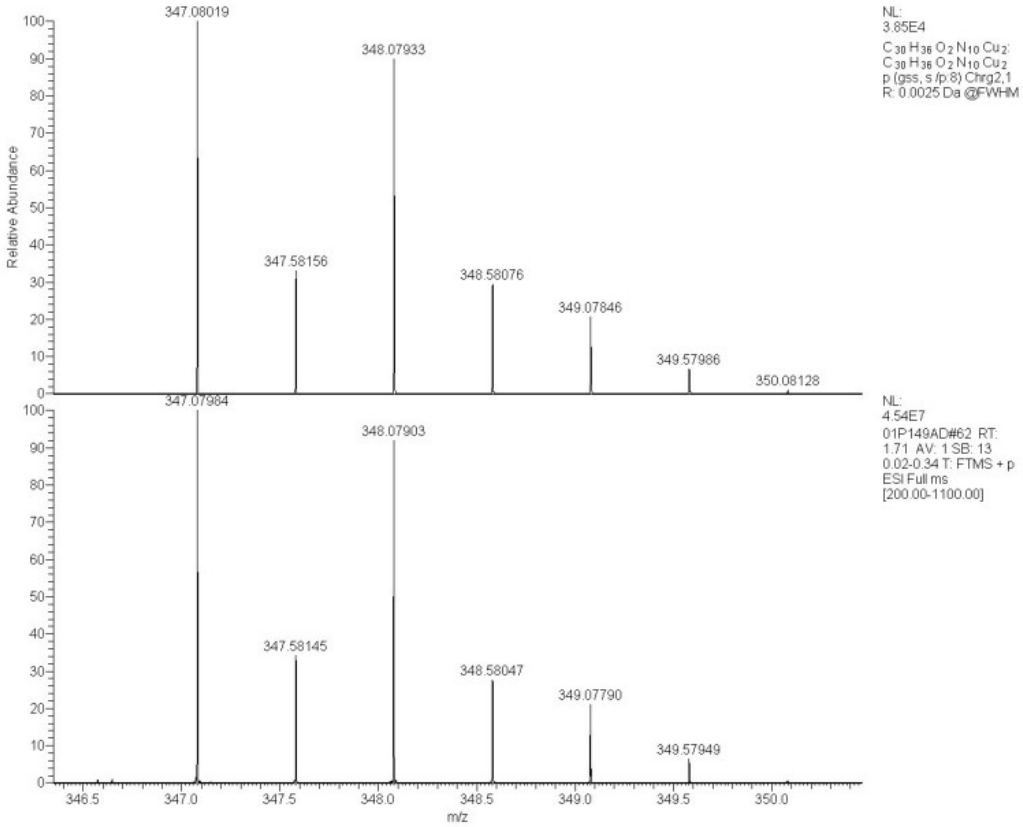

Figure S6. HR-ESI-MS spectrum of **C1·(OTf)$_2$**. Experimental (top) and simulated (bottom) for the [M – 2 OTf]$^{+2}$ cation.

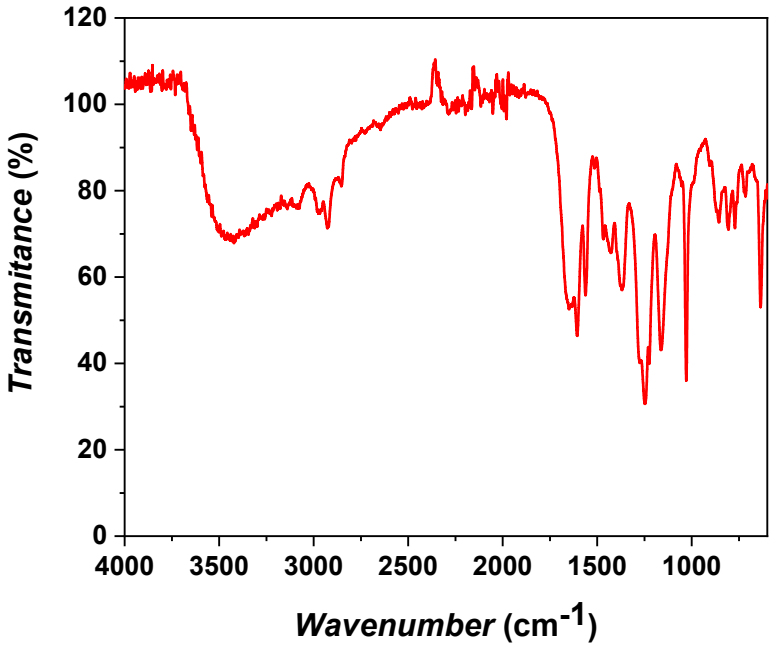

Figure S7. IR-ATR spectrum of **C1·(OTf)$_2$**.

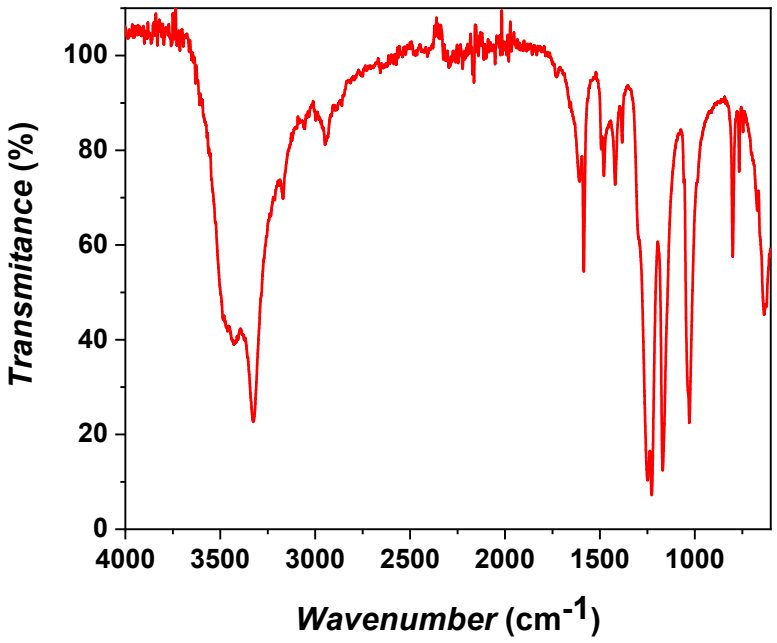

Figure S8. IR-ATR spectrum of **C2**.

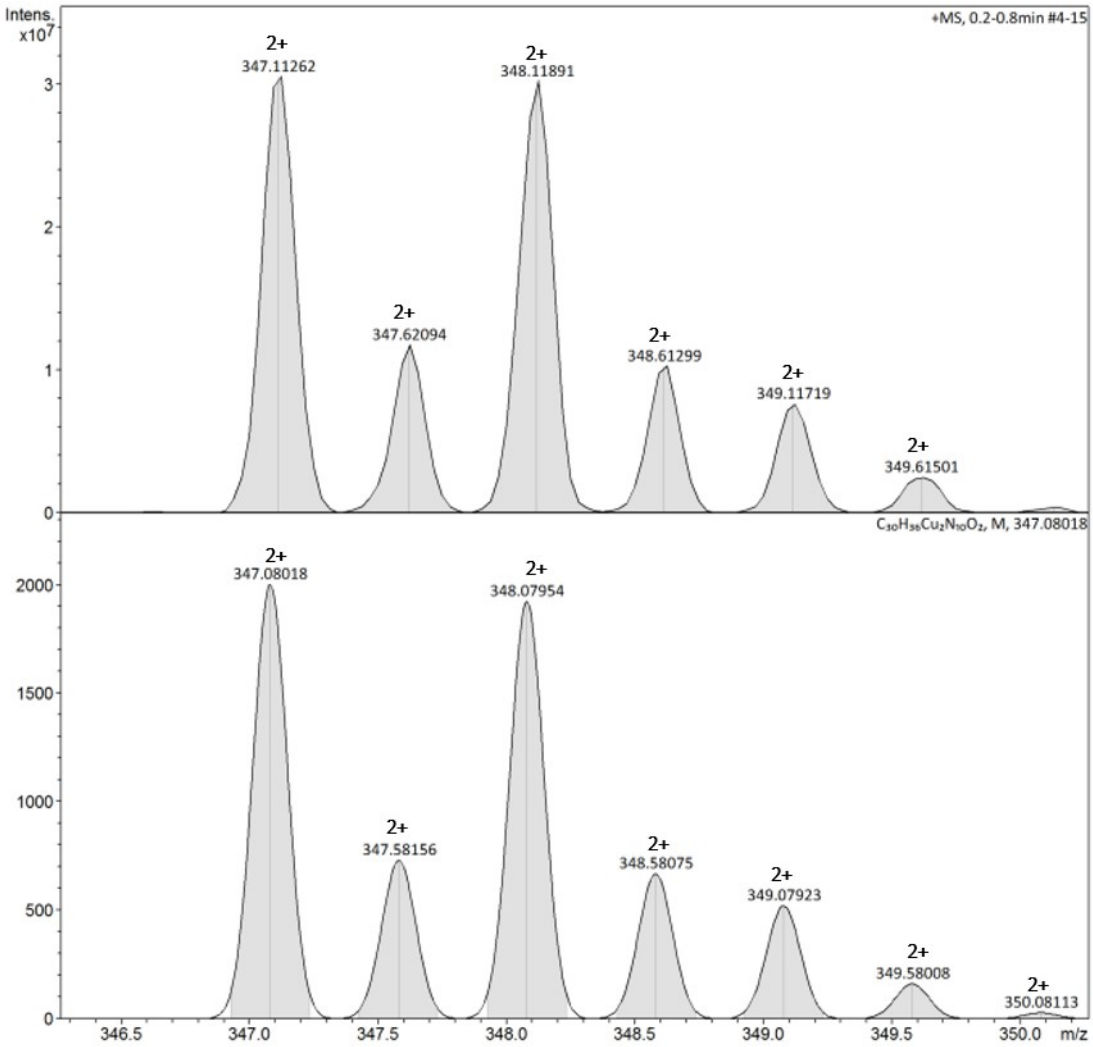

Figure S9. ESI-MS spectrum of **C1·$(BF_4)_2$**. Experimental (top) and simulated (bottom) for the [M – 2 BF_4]$^{2+}$ cation.

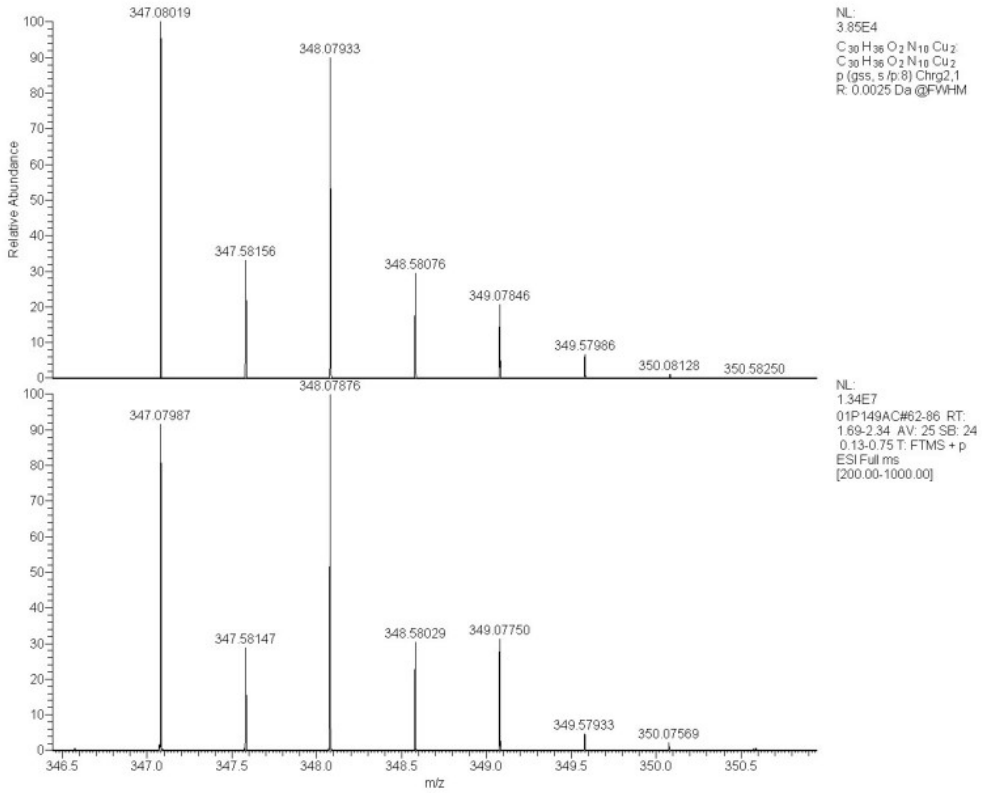

Figure S10. HR-ESI-MS spectrum of **C1·$(BF_4)_2$**. Experimental (top) and simulated (bottom) for the [M – 2 BF_4]$^{2+}$ cation.

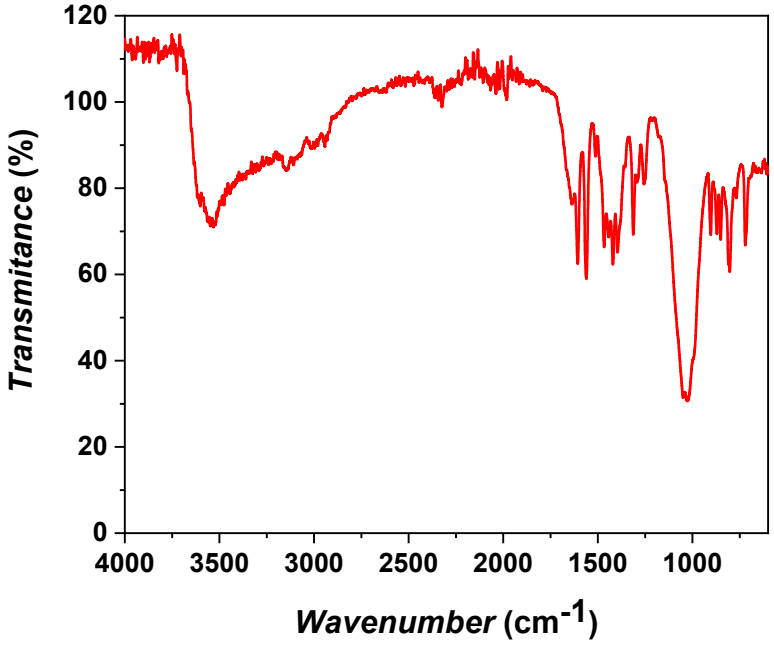

Figure S11. IR-ATR spectrum of **C1·$(BF_4)_2$**.

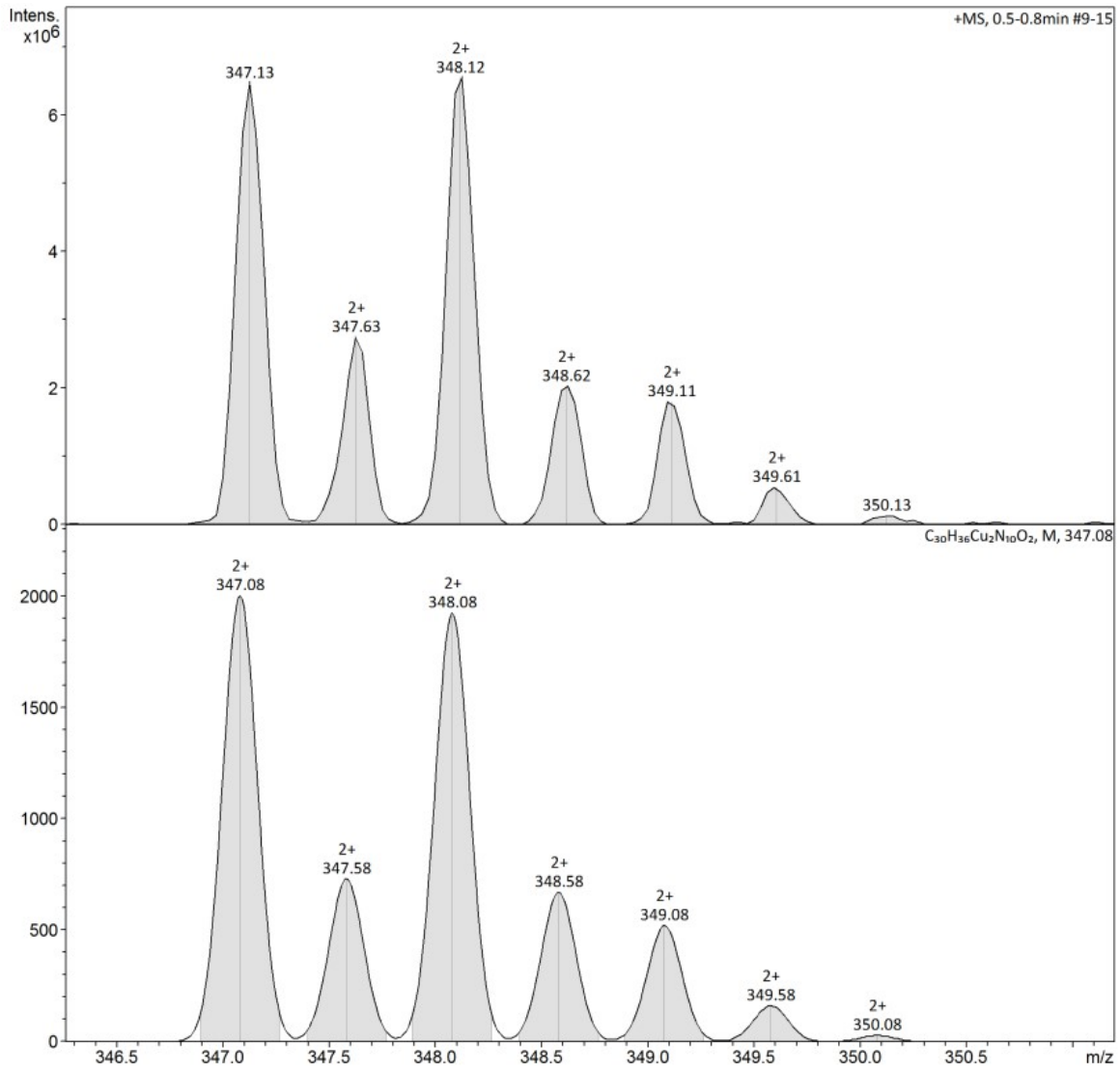

Figure S12. ESI-MS spectrum of **C1·$(ClO_4)_2$**. Experimental (top) and simulated (bottom) for the [M – 2 ClO_4]$^{2+}$ cation.

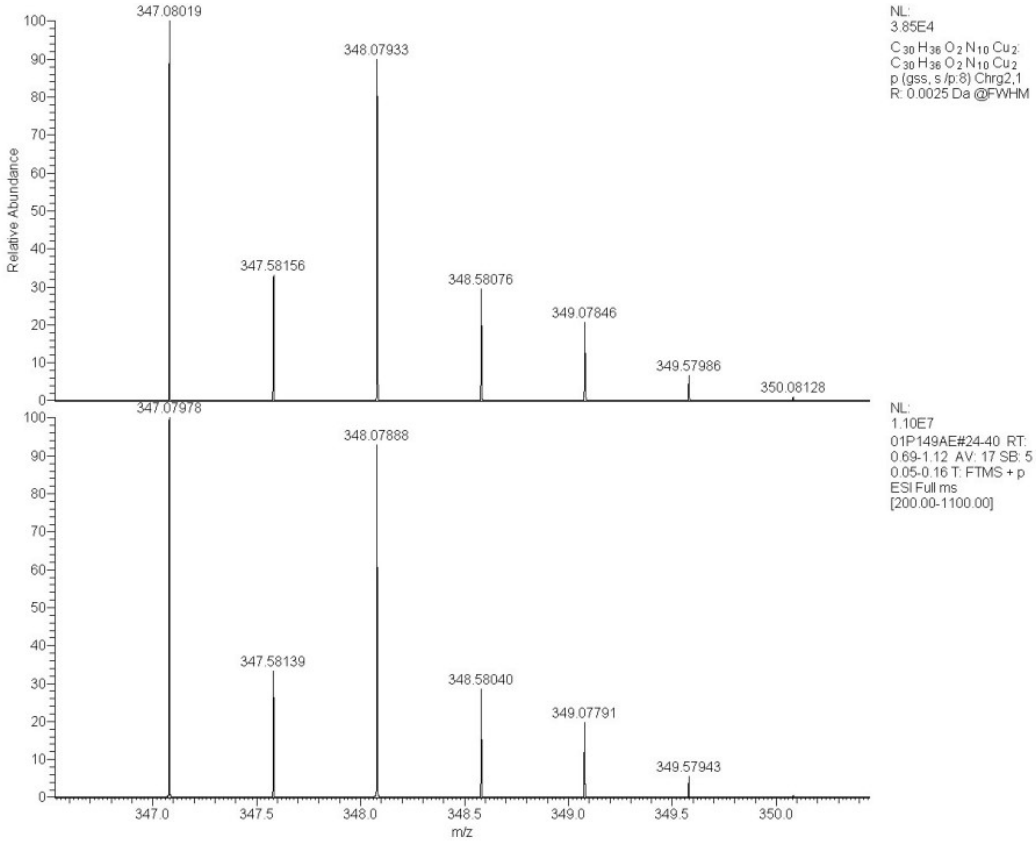

Figure S13. HR-ESI-MS spectrum of **C1·(ClO$_4$)$_2$**. Experimental (top) and simulated (bottom) for the [M – 2 ClO$_4$]$^{2+}$ cation.

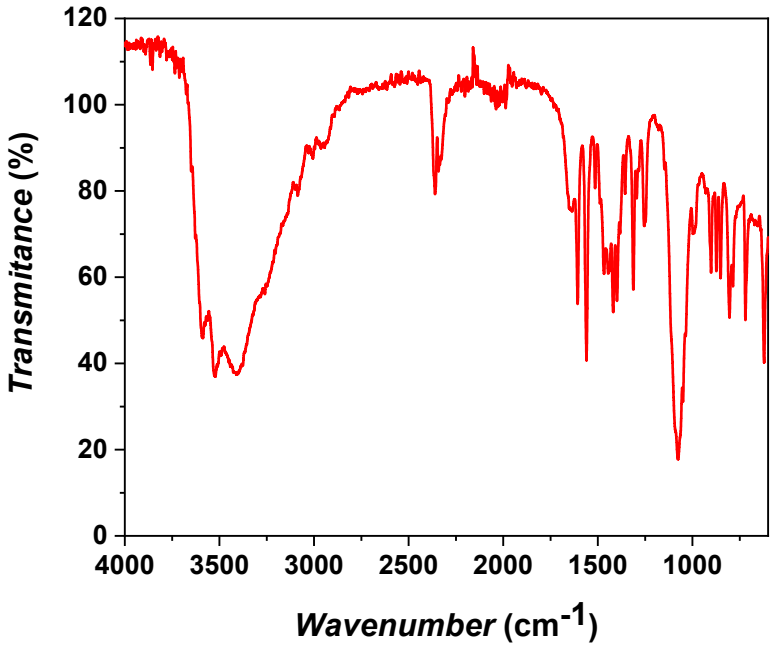

Figure S14. IR-ATR spectrum of **C1·(ClO$_4$)$_2$**.

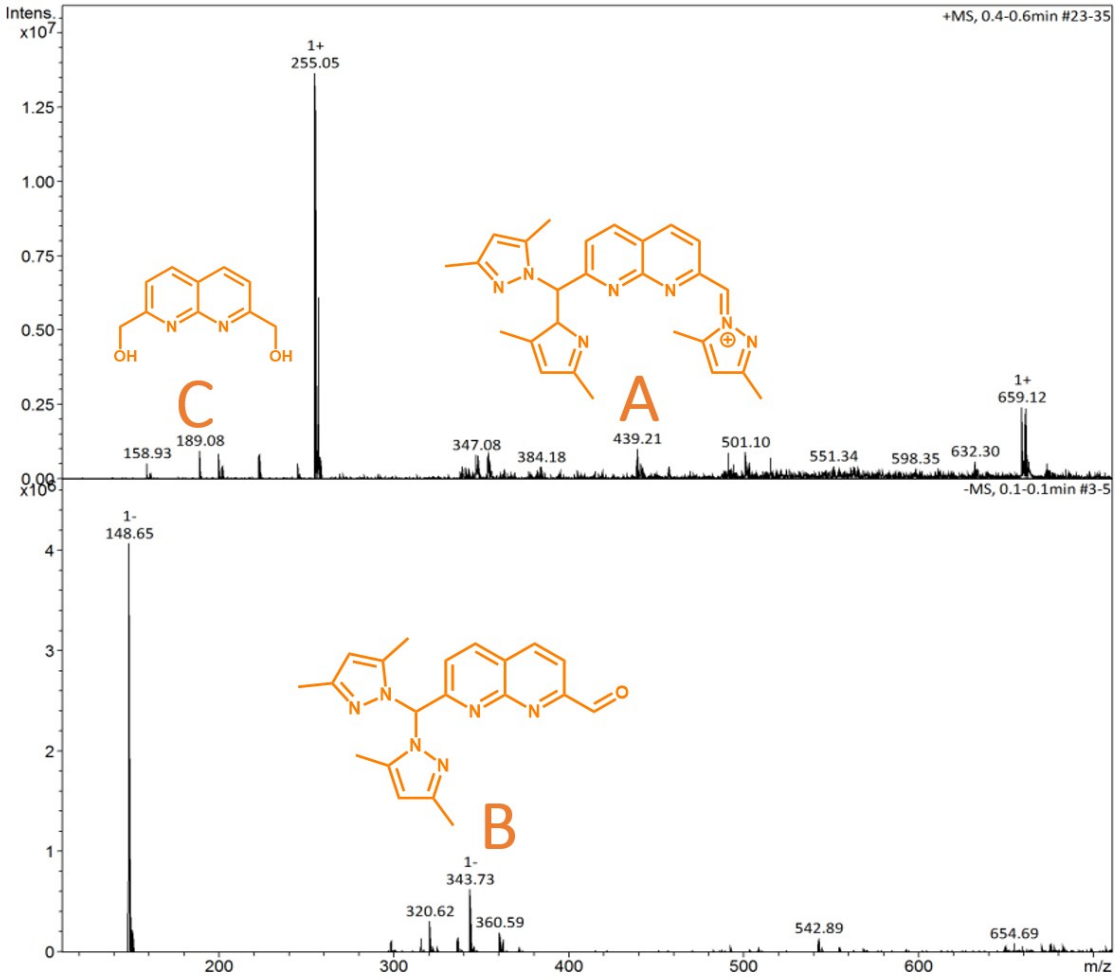

Figure S15. ESI-MS spectrum of the crude solution after the synthesis of **C1·(OTf)$_2$**. Positive (top) and negative (bottom) mode.

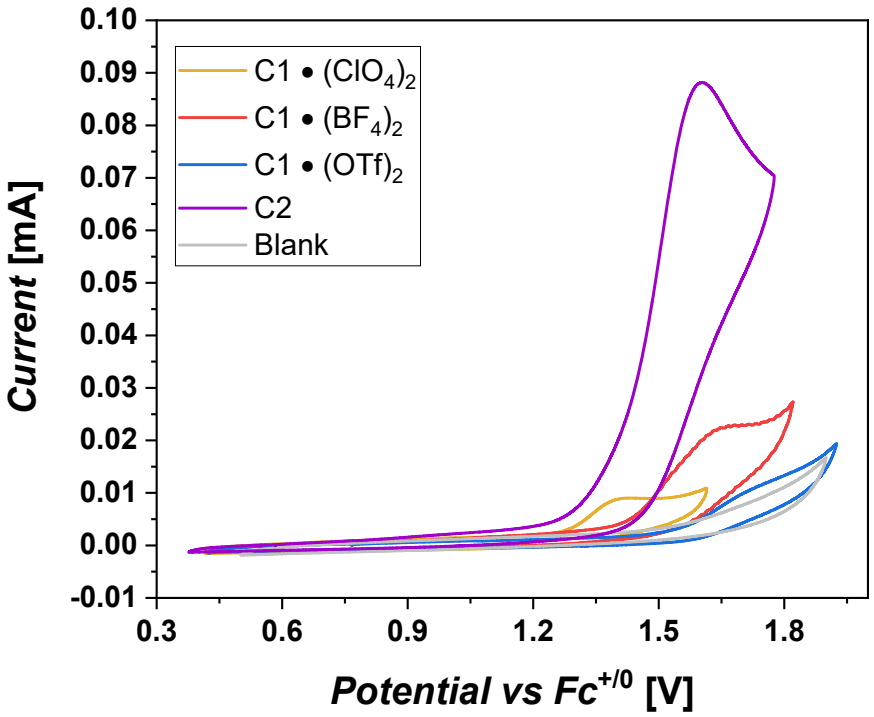

Figure S16. Cyclic voltammograms for 1 mM solutions of **C1·$(ClO_4)_2$** (orange), **C1·$(BF_4)_2$** (red), **C1·$(OTf)_2$** (blue) and **C2** (purple) complexes under Ar-saturated anhydrous acetonitrile containing 0.1 M [*n*-$Bu_4N]ClO_4$. Scan rate = 50 mV s^{-1}.

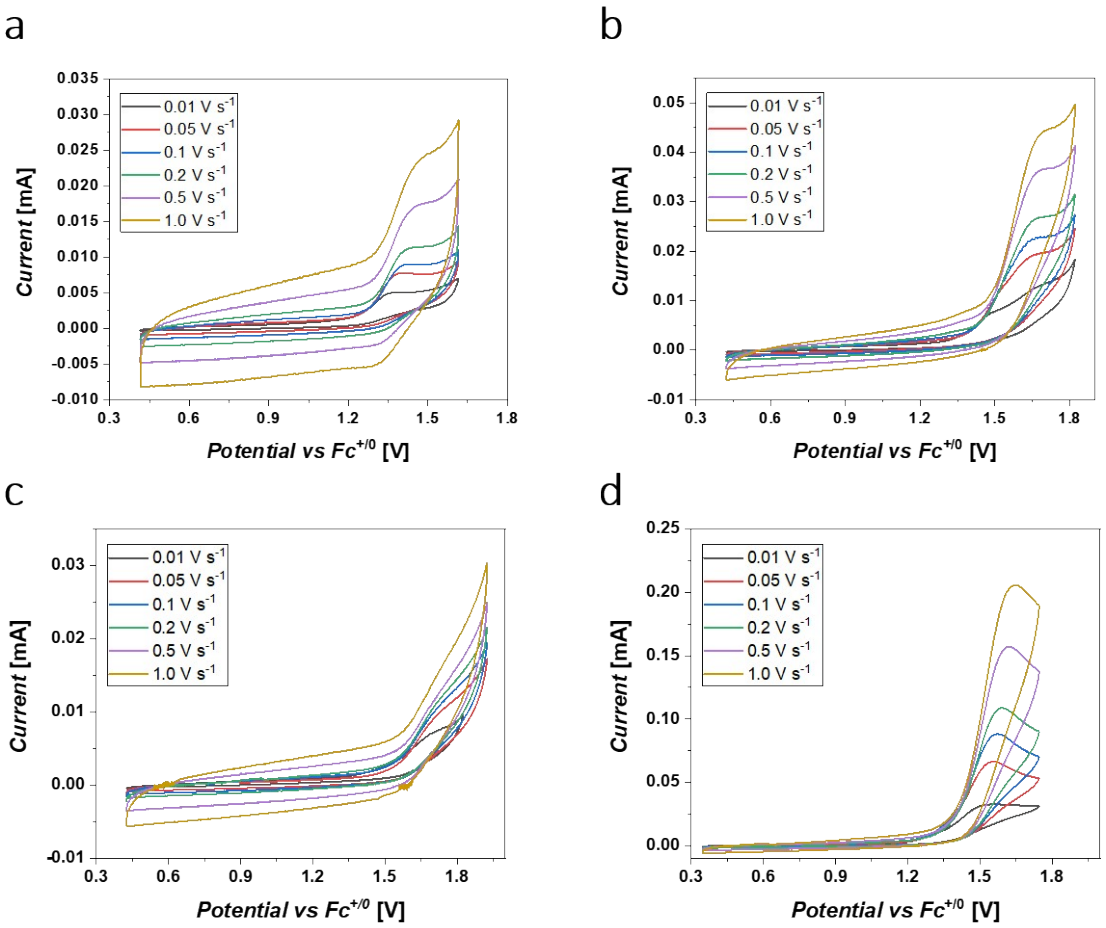

Figure S17. Cyclic voltammograms recorded at different scan rates over a glassy carbon working electrode, of 1 mM solution of a) **C1·(ClO$_4$)$_2$,** b) **C1·(BF$_4$)$_2$,** c) **C1·(OTf)$_2$** and d) **C2** in Ar-saturated anhydrous acetonitrile containing 100 mM [*n*-Bu$_4$N]ClO$_4$.

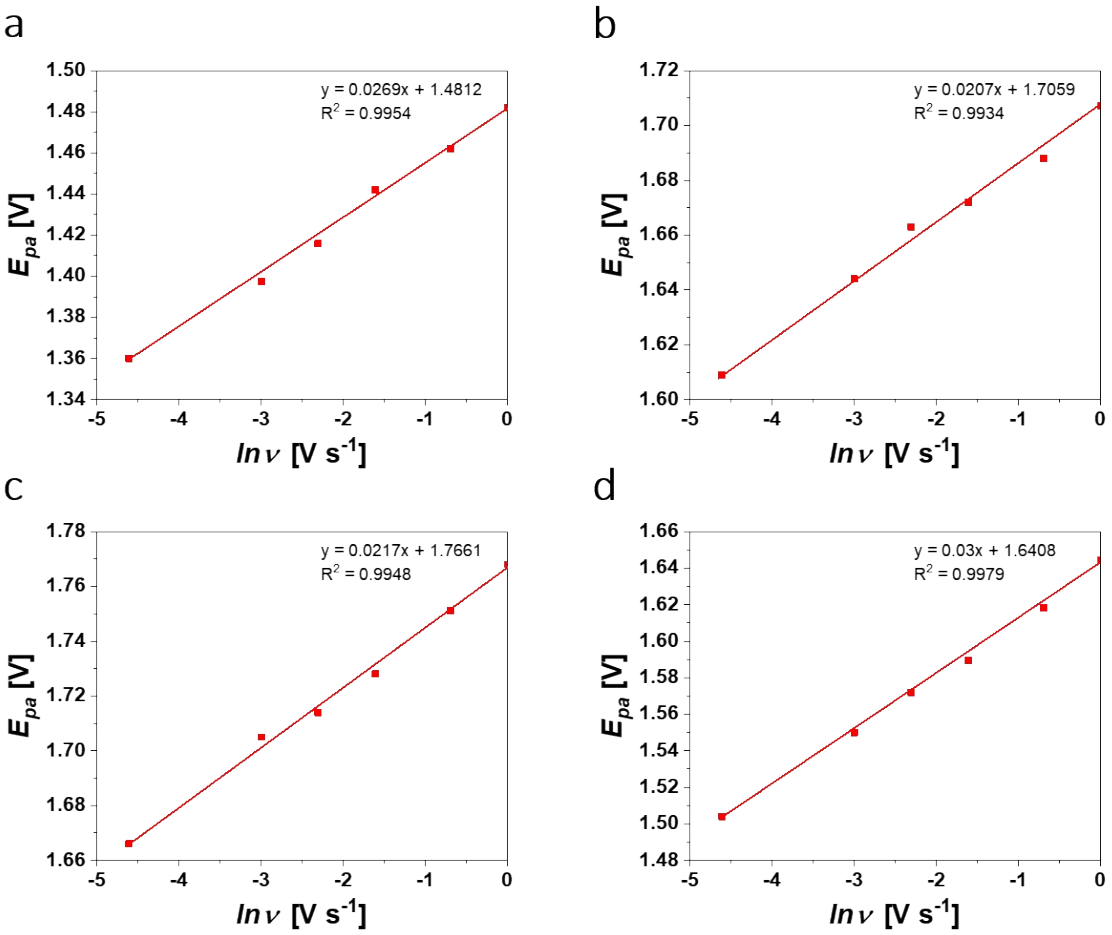

Figure S18. Plots of the E_{pa} associated to the oxidation event vs $ln\ \nu$) of a) **C1·(ClO$_4$)$_2$**, b) **C1·(BF$_4$)$_2$**, c) **C1·(OTf)$_2$** and d) **C2**.

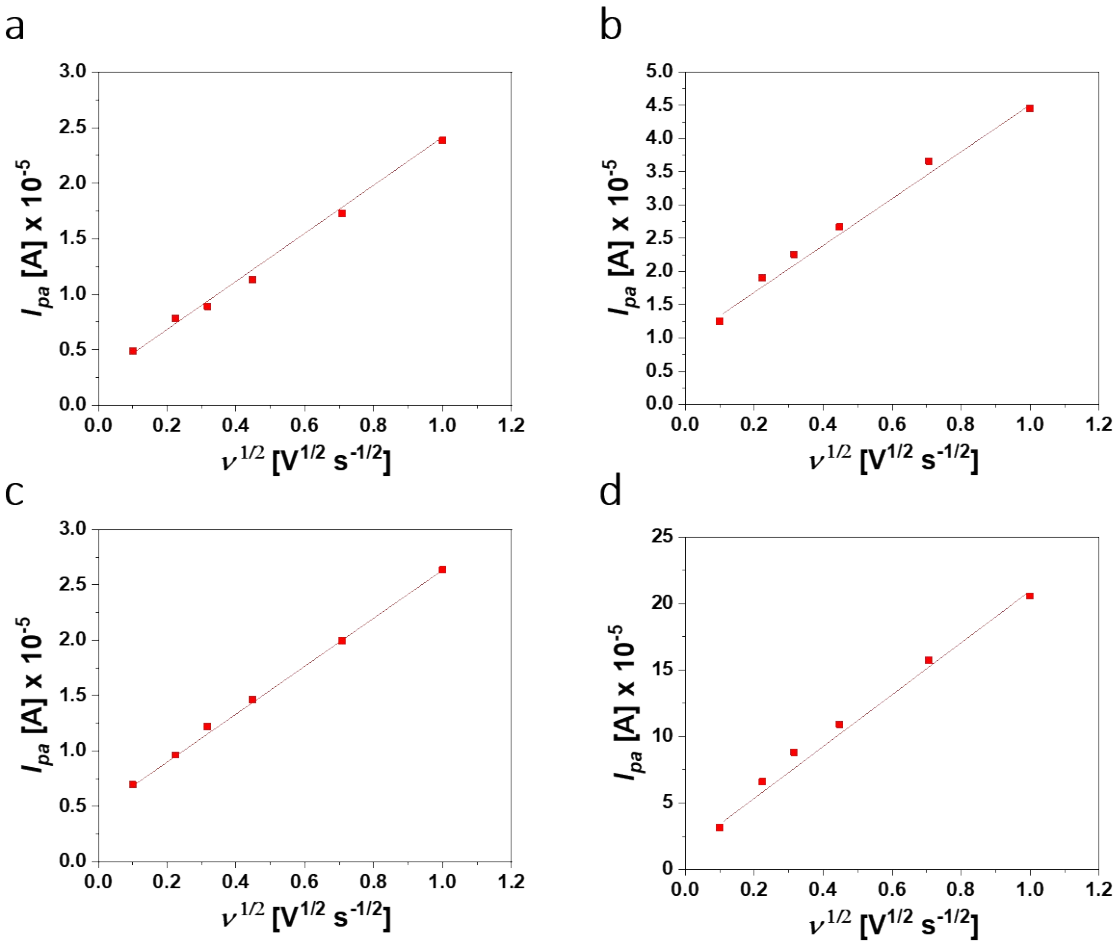

Figure S19. Randles-Ševčik plots of the anodic currents associated to the oxidation potential (I_{pa}) of a) **C1·$(ClO_4)_2$**, b) **C1·$(BF_4)_2$**, c) **C1·$(OTf)_2$** and d) **C2** as function of the square root of the scan rate.

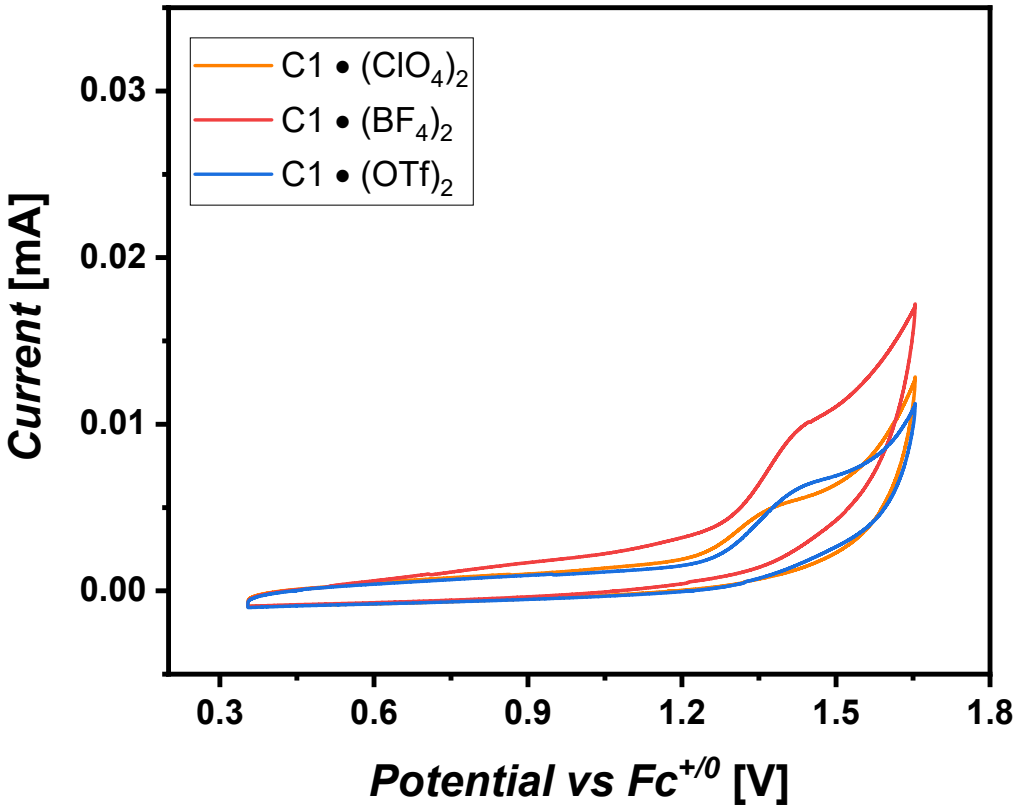

Figure S20. Cyclic voltammograms for 1 mM solutions of **C1·(ClO$_4$)$_2$** (orange), **C1·(BF$_4$)$_2$** (red) and **C1·(OTf)$_2$** (blue) complexes in Ar-saturated anhydrous acetonitrile containing 0.1 M [*n*-Bu$_4$N]BF$_4$. Scan rate = 50 mV s^{-1}.

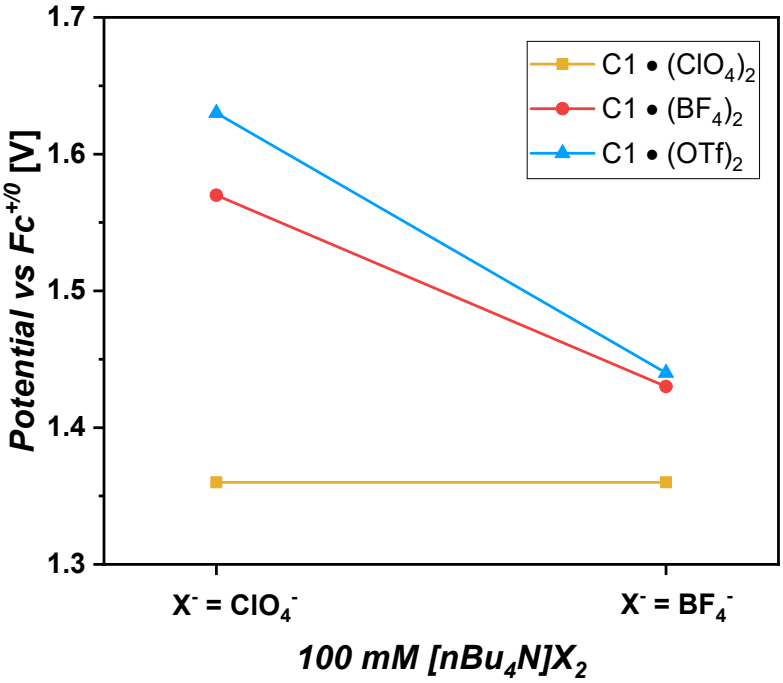

Figure S21. Comparison of E_{pa} for **C1·(ClO$_4$)$_2$** (orange), **C1·(BF$_4$)$_2$** (red) and **C1·(OTf)$_2$** (blue) complexes under 100 mM [nBu$_4$N]ClO$_4$ and [nBu$_4$N]BF$_4$.

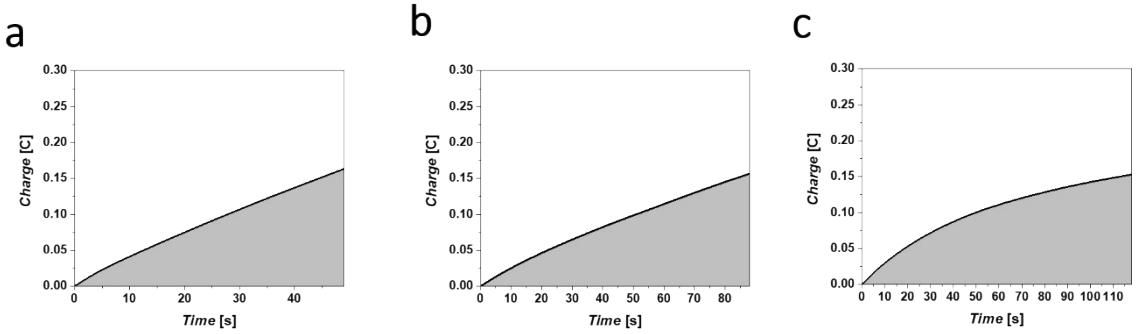

Figure S22. Evolution of the charged passed corresponding to 0.5 mol e$^-$ (*ca.* 0.16 C) for a) **C1·(ClO$_4$)$_2$**, b) **C1·(BF$_4$)$_2$** and c) **C1·(OTf)$_2$** run at 1.49 V vs Fc$^{+/0}$, 1.73 V vs Fc$^{+/0}$ and 1.81 V vs Fc$^{+/0}$, respectively, over a C_{foam} working electrode, in the presence of 3 mL of 1 mM complex solutions in Ar-saturated anhydrous acetonitrile containing 100 mM of [*n*-Bu$_4$N]ClO$_4$.

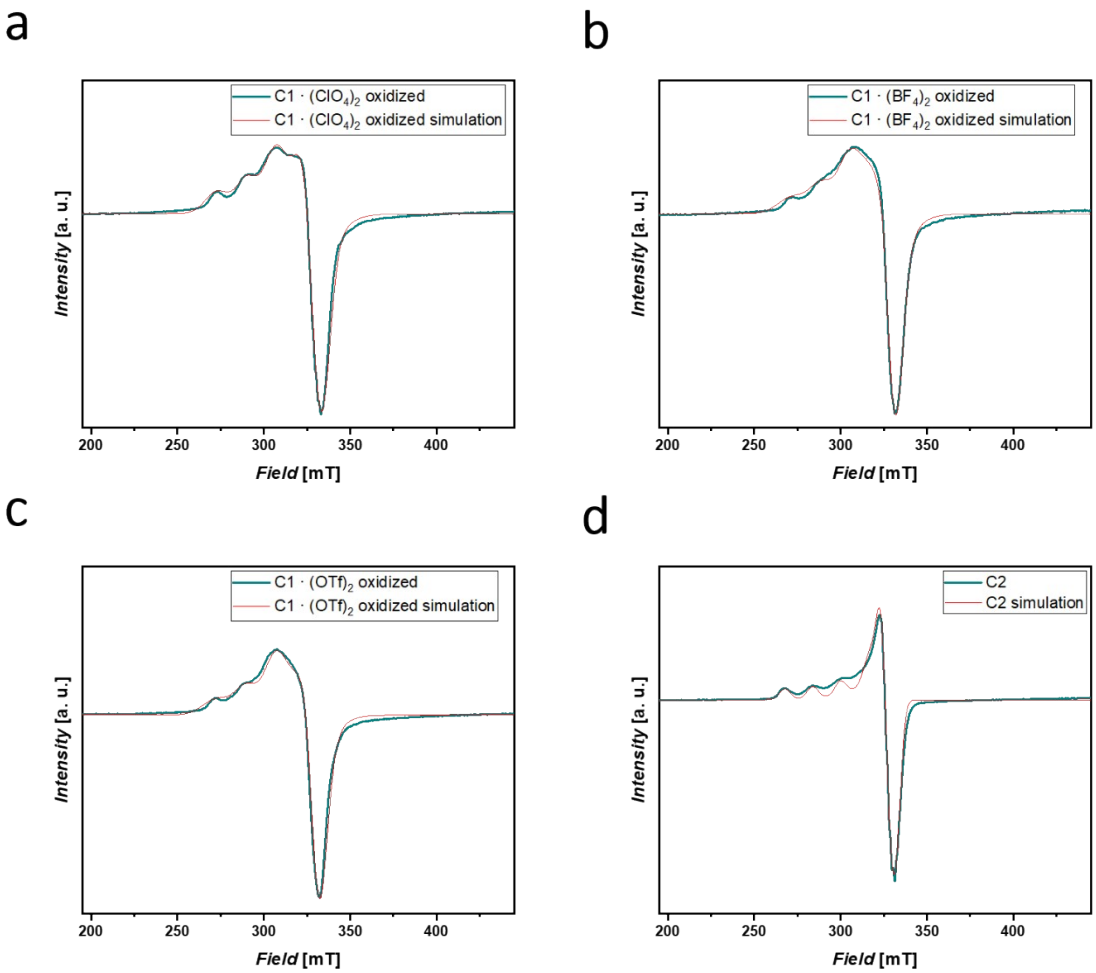

Figure S23. EPR spectra and their simulations for the oxidized complexes a) **C1·$(ClO_4)_2$**, b) **C1·$(BF_4)_2$**, c) **C1·$(OTf)_2$** and d) **C2**.

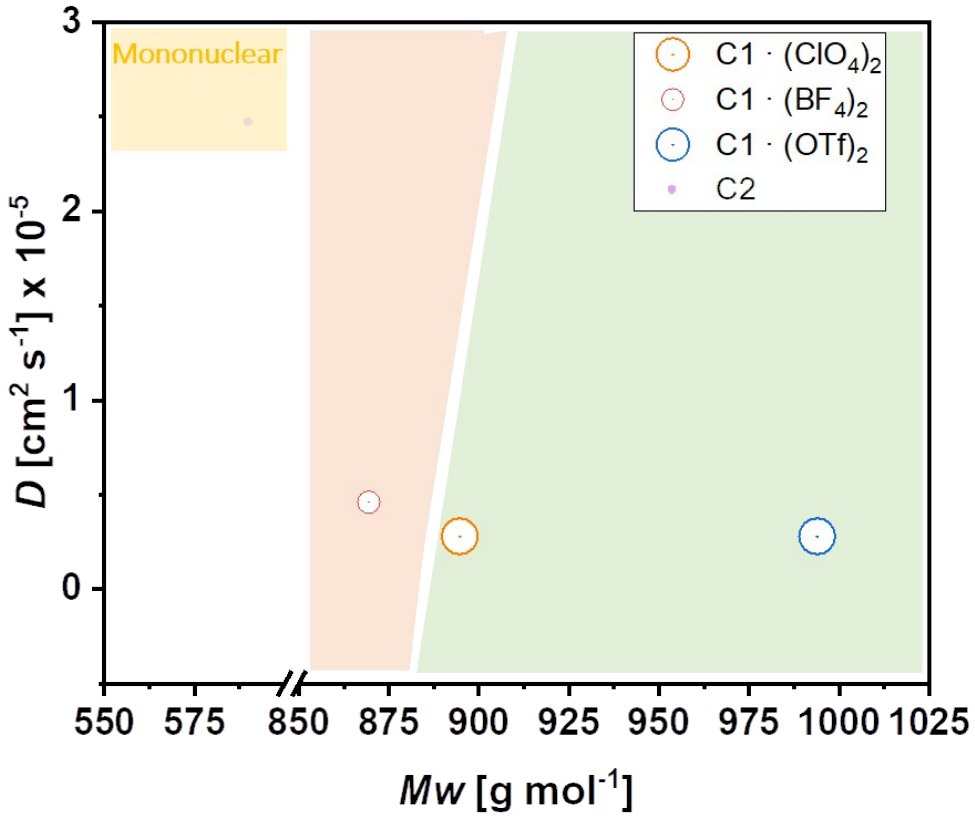

Figure S24. Full range plot of the diffusion coefficients for the different complexes in anhydrous acetonitrile containing 0.1 M [*n*-Bu_4N]ClO_4 at 298 K, against their respective molecular weights. Hydrodynamic radii have been included for comparison purposes.

[1] Stoll, S.; Schweiger, A. *J. Magn. Reson.* **2006**, *178*, 42-55.
[2] Molton, F. *Magn. Reson. Chem.* **2020**, *58*, 718-726.
[3] A. J. Bard, L. R. Faulkner, Electrochemical Methods: Fundamentals and Applications, Wiley, Hoboken, **2001**
[4] Duisenberg, A. J. M.; Kroon-Batenburg, L. M. J.; Schreurs, A. M. M. *J. Appl. Cryst.* **2003**, *36*, 220-229.
[5] Sheldrick, G. M. *Acta Crystallogr.* **2008**, *A64*, 112–122.
[6] Dolomanov, O. V.; Bourhis, L. J.; Gildea, R. J.; Howard, J. A. K.; Puschmann, H. *J. Appl. Crystallogr.* **2009**, *42*, 339–341.
[7] Sheldrick, G. M. *Acta Crystallogr.* **2015**, *71*, 3–8.